MASTERARBEIT / MASTER'S THESIS

Titel der Masterarbeit / Title of the Master's Thesis

The role of GATA6 in the molecular phenotypes of PDAC

verfasst von / submitted by

Vivien-Sandra Ionasz

Angestrebter akademischer Grad / in partial fulfilment of the requirements for the degree of

Master of Science (MSc)

Wien, 2019 / Vienna 2019

Studienkennzahl lt. Studienblatt / Degree programme code as it appears on the student record sheet:	UA 066 606
Studienrichtung lt. Studienblatt / Degree programme as it appears on the student record sheet:	Masterstudium Drug Discovery and Development
Betreut von / Supervisor:	Univ.-Prof. Dr. Verena Dirsch

1 Acknowledgment

First and foremost, I would like to acknowledge Dr. Paola Martinelli for accepting me into her small but amazing research group, giving me the possibility to work on this fascinating project and studying more about a, for me new, cancer type. I gained a lot of deeper insight into the world of research and was able to experience many interesting things during my time in her laboratory. I am grateful for getting guidance while also being able to work independently, this way I was able to grow as a researcher and also as a person. Additionally, I appreciate the patience, feedback, advice, and support of the whole lab. Thank you, Berni, and thank you, Denise! I could not have done it without you. I would also like to thank everyone who is part of the Institute of Cancer Research for treating me as an equal. It was a pleasure to work with you and to learn new things from all of you.

Finally, I want to also thank my family and my friends, old and new, for encouraging me throughout the year to go beyond my comfort zone and to follow my dreams. The last year was a hell of a ride, but with your continuous help and support, I did everything that I needed to do and more. I will forever be thankful for that!

2 Declaration of Authorship

I declare that this Master Thesis has been written by myself. I have not used any other than the listed sources, nor have I received any unauthorized help.

I hereby certify that I have not submitted this Master Thesis in any form (to a reviewer for assessment) either in Austria or abroad.

Furthermore, I assure that the (printed and electronic) copies I have submitted are identical.

Date: 24.09.2019 Signature: .....

3 Abstract

No big advances have been made in the treatment of pancreatic cancer, which still has a five-year survival rate lower than 5%, during the last decades. The transcription factor GATA6 was linked to the classical subtype of pancreatic ductal adenocarcinoma (PDAC) and the more aggressive subtypes were observed to have lower GATA6 expression levels. ΔNp63, a short isoform of the tumor protein TP63 which acts tumor-promoting, was linked to the basal-like subtype and to epigenetic changes favoring it. This study aims to elucidate the relationship between GATA6 and ΔNp63 in the context of the molecular phenotypes. The possible role of GATA6 in the regulation of epigenetics should be explored, in addition to analyzing whether GATA6 inhibits the ΔNp63-driven basal phenotype in PDAC. Based on two GATA6-overexpressing cell lines and one knockdown model, the alterations in protein and gene expression, proliferation, migration, invasion as well as chromatin landscape were evaluated. In one of the overexpression models, namely the BxPC-3 cell line, GATA6 was able to downregulate ΔNp63 and a part of the basal-like program, however, no association to epigenetic changes were established. Interestingly, also a discrepancy between the basal-like subtype and EMT was observed, suggesting that these are two different concepts. Based on these results we can conclude with two out of three models that GATA6 and ΔNp63 have an indirectly proportional relationship. However, context-dependency would need to be further investigated since the GATA6-overexpression L3.6pl cells showed an increase in ΔNp63 instead.

4 Kurzfassung

Bei der Behandlung von Bauchspeicheldrüsenkrebs, bei dem die Fünfjahresüberlebensrate immer noch unter 5% liegt, wurden keine großen Fortschritte innerhalb der letzten Jahrzehnte erzielt. Der Transkriptionsfaktor GATA6 wurde mit dem klassischen Subtyp des duktalen Adenokarzinoms der Bauchspeicheldrüse (PDAC) in Verbindung gebracht, und es wurde beobachtet, dass die aggressiveren Subtypen niedrigere Expression an GATA6 aufwiesen. ΔNp63, eine tumorfördernde kurze Isoform des Tumorproteins TP63, wurde mit dem basalähnlichen Subtyp und den ihn begünstigenden epigenetischen Veränderungen in Verbindung gebracht. Diese Studie zielt darauf ab, die Beziehung zwischen GATA6 und ΔNp63 im Kontext der molekularen Phänotypen aufzuklären. Die mögliche Rolle von GATA6 bei der Regulation der Epigenetik sollte untersucht werden. Außerdem sollte untersucht werden, ob GATA6 den ΔNp63-getriebenen basalen Phänotyp in PDAC hemmt. Basierend auf zwei GATA6-überexprimierenden Zelllinien und einem Knockdown-Modell wurden die Veränderungen der Protein- und Genexpression, der Proliferation, der Migration, der Invasion sowie der Chromatinlandschaft analysiert. In einem der Überexpressionsmodelle, nämlich der BxPC-3-Zelllinie, war GATA6 in der Lage, ΔNp63 und einen Teil des basalähnlichen Programms runter zu regulieren, es wurde jedoch kein Zusammenhang mit epigenetischen Veränderungen festgestellt. Interessanterweise wurde auch eine Diskrepanz zwischen dem basalartigen Subtyp und dem EMT beobachtet, was darauf hindeutet, dass es sich um zwei verschiedene Konzepte handelt. Basierend auf diesen Ergebnissen können wir mit zwei von drei Modellen schließen, dass GATA6 und ΔNp63 eine indirekt proportionale Beziehung haben. Die Kontextabhängigkeit müsste jedoch weiter untersucht werden, da die GATA6-Überexpression in L3.6pl-Zellen stattdessen einen Anstieg von ΔNp63 aufwies.

5 Table of contents

6 Introduction

6.1 PDAC

Cancer is slowly but steadily becoming the number one killer of humans. According to the World Health Organization, it represents nowadays the second leading cause of death worldwide[1]. One particularly lethal type of cancer with a dismal prognosis is pancreatic cancer. For 2018 the International Agency for Research on Cancer estimated 458,918 incidences and 432,242 mortalities for pancreatic cancer alone[2]. In general, the 5-year survival rates of pancreatic cancer are reported to be as low as 3%, since diagnosis is usually given at an already advanced stage of the disease[3]. In Figure 1, pancreatic cancer can be seen at the lower end of the 5-year cancer survival rates in comparison to many other cancer types with a better prognosis. Another notable remark is that also when comparing the survival rates between 1975 and 2003 no big improvement was being made in improving the life expectancy of patients with pancreatic cancer.

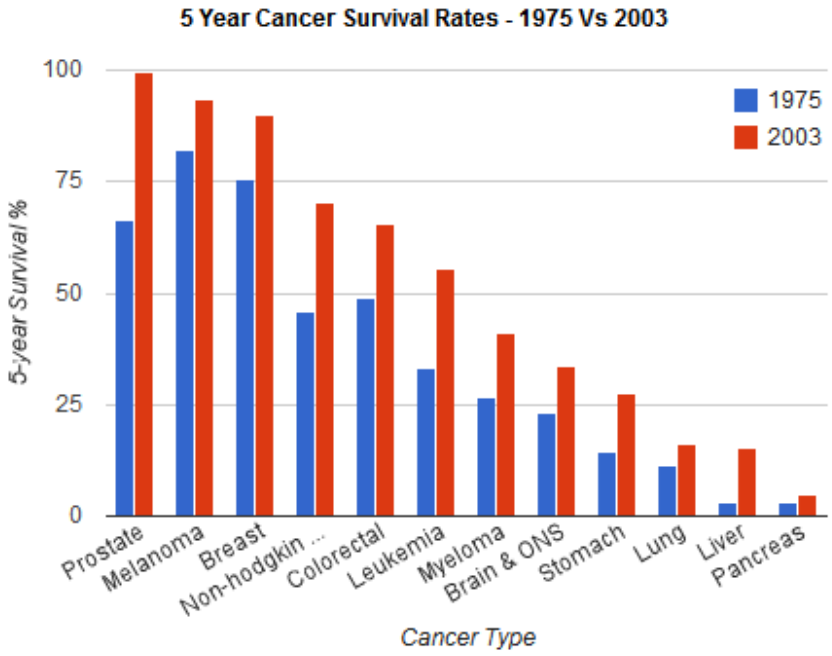

Figure 1: Comparison of 5-year cancer survival rates of different cancer types between 1975 and 2003. Figure retrieved from http://healthhubs.net/images/cancer-survival-trends.gif [4].

Pancreatic ductal adenocarcinoma (PDAC) is a tumor that arises from the exocrine part of the pancreas. It is also the predominant type of pancreatic cancer and develops from non-invasive precursor lesions, which are usually referred to as pancreatic intraepithelial neoplasias (PanINs). The most frequently mutated gene in PDAC, which is mutated in more than 95% of the patients, is KRAS. Two variants, namely KRAS G12D or G12V, are recurrent and both lock KRAS in a constitutively active state continuously signaling downstream into the MAPK and Akt pathways. Therefore, KRAS is known as the driver mutation of PDAC, however, this mutation is necessary but not sufficient for the initial development of PDAC from PanINs[5]. Various mouse models have been established to study PDAC's initiation and progression[6]. The most widespread genetically engineered mouse models (GEMM) for pancreatic cancer are based on the expression of oncogenic KRAS[7]. One of them, the KPC model has been first described in 2005[8] and harbors in addition to a mutated KRAS^{G12D} allele, a heterozygous p53 mutation (R172H) and expression of Pdx-1-Cre. The mutated alleles of both, KRAS and p53, have STOP cassettes in front of the first exon, which is only removed by tissue-dependent expression of Pdx1-Cre, which is starting to be expressed during the embryonic development of the pancreas. This leads to the conditional tissue- and time-specific expression of the oncogenes. However, even though the mutational burden is not high, the disease progresses very fast in this model and 16-week-old mice have already developed invasive PDAC due to the early initiation with KRAS and p53 mutations[8,9].

When generating these KRAS-driven models, it became clear that in addition to the constitutively active KRAS, additional tumor suppressor losses need to take place for the disease to develop in mice[5]. During the transition from the lesions to PDAC, various genetic aberrations are taking place, such as the loss of *CDKN2A, TP53*, and *SMAD4*[10]. During this process, also histological changes are evident: in the three different stages prior to the final tumor formation (PanIN1 to PanIN3) an increase in the cellular and nuclear atypia is visible[5] (Figure 2). One event that also seems to take place during PDAC progression in a subset of cases is the loss of *GATA6*, which was first described as an amplified oncogene due to copy number gains[11–13].

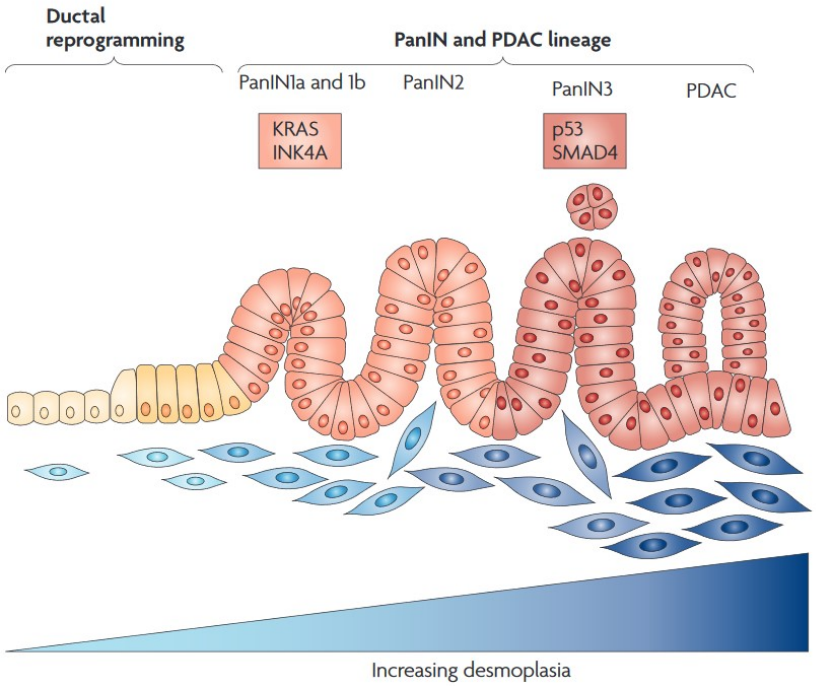

Figure 2: Development of the tumor from non-invasive precursor lesions (PanINs) with early genetic aberrations indicated. Figure adapted from Morris, J. P., Wang, S. C., & Hebrok, M. (2010)[5].

Another important part of PDAC is its complex stromal involvement. As the PanINs progress to PDAC and the cellular morphology changes, also increased desmoplasia is taking place. Fibrous and connective tissue, known as the stroma, is growing more around the tumor. Different cell types such as cancer-associated fibroblasts, immune cells, and blood vessels can be found around the tumor cells. Remarkably, stromal components can account for up to 90% of pancreatic tumors[14]. This tumor microenvironment can hinder the delivery of drugs to the intended cells of the tumor as well as change the tumor's therapeutic response. Therefore, an additional focus was set on tumor-stroma interactions in the last years[15]. It has been thought that by removing the stroma better delivery of chemotherapy is possible. However, interestingly two studies[16,17], which have been published together, showed that the total depletion of stroma around the tumor tissue led to a more aggressive phenotype with dedifferentiated cells that were proliferating faster. This demonstrated that the stroma is not only aiding the growth of the tumor but also inhibiting it simultaneously, making its interactions more complex than initially thought[16]. Trying to find an approach that is not depleting the whole tumor microenvironment while also targeting tumor cells seems to be the right approach in the case of PDAC. Nevertheless, finding the equilibrium between these two strategies is problematic, since fibrosis is negatively impacting drug treatment while angiogenesis could benefit getting the drug to its intended location[14].

6.2 Treatment

Even though different therapies and screening methods were developed in the last years, there was no real improvement in survival (compared to other cancer types) while the incidence rate is still increasing [18]. Normally patients are treated with chemotherapy for advanced and metastatic tumors. Some unresectable, metastatic cancers might be treated with a combination of chemotherapy and radiation, while resectable tumors will be surgically removed in addition to adjuvant therapy. This is however based on localization of the tumor and its extension, as well as the patient's performance status[19].

5-Fluorouracil (5-FU) (Figure 3) was, despite its toxicity, one of the first treatment options in pancreatic cancer, since it showed moderate efficacy in improving patient's life[18]. The mode of action of this compound is that it is an antimetabolite and pyrimidine analog, which stops the production of new DNA by blocking the enzyme thymidylate synthase, leading to cell death[20].

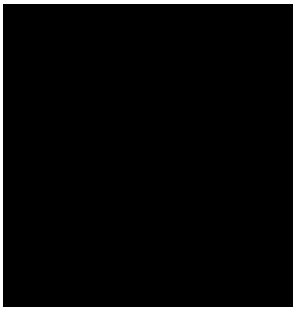

Figure 3: Structure of 5-fluorouracil.
Figure retrieved from https://upload.wikimedia.org/wikipedia/commons/9/9b/Fluorouracil2DACS.svg[21].

Gemcitabine is a first-line therapy for patients with good performance status, which means that the patient is not bedridden and can still perform basic activities alone. However, the improvement in median survival time was relatively low with 5.6 months, compared to 4.4 months for 5-FU[22]. The mechanism of action of gemcitabine is based on it being a nucleoside analog. With its chemical structure, see **Fehler! Verweisquelle konnte nicht gefunden werden.**, it is blocking the synthesis of new DNA, which results in subsequent cell death, which is, as with all chemotherapeutic drugs, not specific to cancer cells but to cycling cells[23].

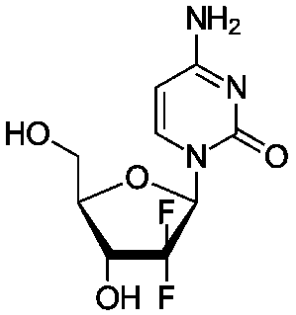

Figure 4: Structure of gemcitabine.
Figure retrieved from https://upload.wikimedia.org/wikipedia/commons/f/ff/Gemcitabine.svg[24].

Currently, the state-of-the-art therapy for metastasized PDAC is a combination therapy of FOLFIRINOX (irinotecan, oxaliplatin, 5-fluorouracil and leucovorin, Figure 5). In comparison to gemcitabine a statistically significant improvement is observable (overall survival: 11.1 vs. 6.8 months; progression-free survival: 6.4 vs. 3.3 months), however, the treatment shows an unfavorable safety profile constraining the use to patients under the age of 75 and with good performance status[25]. Nab-paclitaxel plus gemcitabine (Figure 6) is another therapy usually applied in metastatic PDAC. In a phase III clinical trial, again compared to gemcitabine as a monotherapy, there was a substantial increase observable in the overall survival as well as in the progression-free survival. Again, the response rate

improved with this combination therapy. The side effects, similar to the FOLFIRINOX profile, are tolerated on the basis of the enhanced efficacy[26].

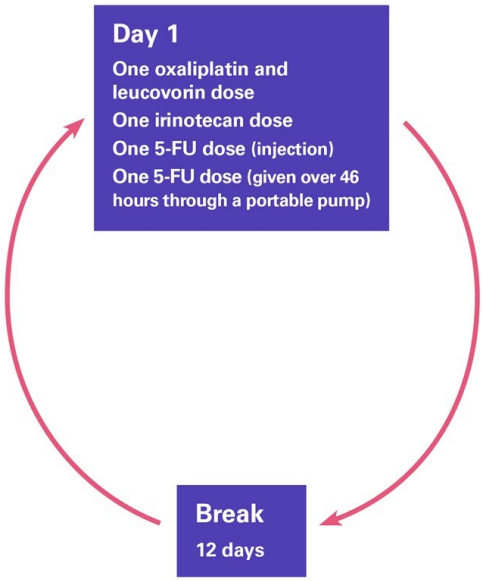

Figure 5: Therapy scheme for FOLFIRINOX.
Figure retrieved from https://www.pancreaticcancer.org.uk/media/1119548/folfirinox-chemotherapy-cycle.jpg[27].

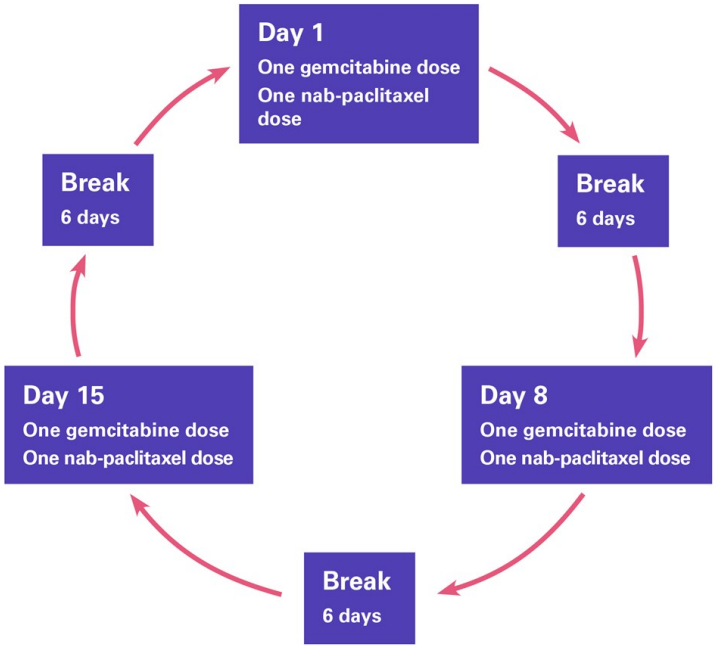

Figure 6: Therapy scheme for nab-paclitaxel plus gemcitabine.
Figure retrieved from https://www.pancreaticcancer.org.uk/media/1119552/oxaliplatin-with-5-fu-and-folinic-acid-folfox-chemotherapy-cycle.jpg[28].

KRAS mutations are the most prevalent mutations in PDAC, they have been linked to PanIN1 initiation and the subsequent progression to cancer[29]. Additionally, in mouse experiments, in which oncogenic KRAS was inducible, tumor shrinkage could be observed[30]. Inhibition of KRAS protein farnesylation did not yield the expected outcomes in trials, however, there is ongoing research to target KRAS directly. Nonetheless, the downstream pathways, such as the MAPK, the mTOR and the PI3K pathways, were explored more in detail[31]. Different kinase inhibitor compounds were developed and tested, but

unfortunately with no increase in overall survival[18]. EGFR, which is the receptor upstream of the KRAS kinase, is often harboring aberrations in pancreatic cancer as well. Erlotinib, an EGFR inhibitor, in combination with gemcitabine, improved the overall survival of patients only moderately[32]. Another option was the use of cetuximab, an anti-EGFR antibody, the results of past phase I trials did not show any survival benefit[33].
Angiogenesis has also been selected as a prominent target in cancer research since it has a pivotal role in the growth of the tumor, as well as in its progression. The clinical trials of the inhibitor axitinib[34,35] and the antibody bevacizumab[36] in pancreatic cancer did not provide any benefit compared to gemcitabine alone.
Immunotherapy was shown to be very efficient in various advanced cancer types. These trials include immune checkpoint inhibitors targeting programmed death receptor 1 (PD-1) and its ligand PD-L1, these pathways are involved in the suppression of the immune system during the carcinogenesis[37]. The use of PD-1 and PD-L1 leads to T cell-mediated killing of tumor cells[38]. Nevertheless, preliminary data on various pancreatic cancer trials did not show any significant improvement until now. Targeting CD40, a member of the tumor necrosis factor family expressed by immune cells, is hypothesized to help overcome the immunosuppressive activity of the stroma by accumulating tumor-suppressive macrophages, which subsequently lead to tumor regression. Currently, a combination of gemcitabine and a CD40 agonist antibody is tested in clinical trials[39,40]. In general, a lot of research progress has been made in recent years, most of the studies are ongoing, therefore conclusions cannot be drawn yet for the newest developments, as for example CAR T (chimeric antigen receptor T) cell therapy[18].

Additional ongoing experimental evaluations include for example inhibition of Hedgehog (HH) signaling, nanoliposomal formulations to achieve higher levels of the used drugs in the blood, as well as drugs targeting the cancer cells' metabolism. The inhibition of HH is based on the preclinical work that linked the cancer cells to the promotion of desmoplasia by signaling via Sonic Hedgehog (SHH) and CXC-motif chemokine receptors[41]. By inhibiting the HH pathway the stromal overgrowth should be decreased, however, the efficacy of HH inhibition in the human could not be validated in a randomized, placebo-controlled trial[42]. This is very complex as the stroma has been linked with different biological functions in PDAC as to promote and inhibit the growth of the tumor, simultaneously, as mentioned above[41].
One nanoliposomal formulation of irinotecan, MM-398, which is currently being tested, acts as a cytotoxic agent and shows an improvement in median survival when used in combination with 5-FU and folinic acid as a second-line therapy during a randomized trial[41,43].
Drugs, which are targeting the metabolism could be very effective due to the deregulated glycolysis and autophagy in cancer. At the same time, the side effects could be excessive when targeting wildtype metabolic enzymes, therefore mutations of the metabolic pathways should be rather targeted. Currently, the anti-malaria treatment hydroxychloroquine, which is also an autophagy inhibitor, is tested in clinical trials in combination with nab-paclitaxel plus gemcitabine in the neoadjuvant setting[44,45], as well as in metastatic pancreatic cancer[46,47].

Pancreatic cancer could be treated with epigenetically active modifiers[48–51], also known as epidrugs, since the majority of factors that seem to be responsible for the development into different subtypes are based on epigenetic nature[52–55] and therefore most probably reversible[56–58]. The first studies focused on HDAC and BET inhibitors, which target enzymes recognizing acetylation marks on the chromatin; by inhibiting these enzymes the transcriptional activity is suppressed[55]. However, the pitfall of today's epidrugs is that they lack specificity and affect the whole genome. With further research, especially the deciphering of epigenetic mechanisms and the discovery of new targets, the development of specific and more efficient epigenetic therapy options could be made possible. In the case of PDAC, also the heterogeneity of the tumors should be taken into consideration, shifting the treatment options more into a personalized therapy approach as well[59].

6.3 Molecular subtypes

Several studies classified PDAC into different categories based on their gene expression profile. Although each study defined slightly different PDAC subtypes, they all agreed on the identification of a subtype with remarkably worse outcome, which was called "quasi-mesenchymal"[60], "basal-like"[11], "squamous"[52] or "pure basal"[61] depending on the study. This specific subtype, which showed overlapping transcriptional profile across the different definitions[62] is correlating with aggressive tumor features and, consequently, poor overall survival, however, it showed to have a better initial response to adjuvant therapy[11,52,60]. Based on the abundant number of clinical trials that are failing for pancreatic cancer[18], this classification could be beneficial to select a patient population with PDAC which is sensitive to a particular treatment[63].

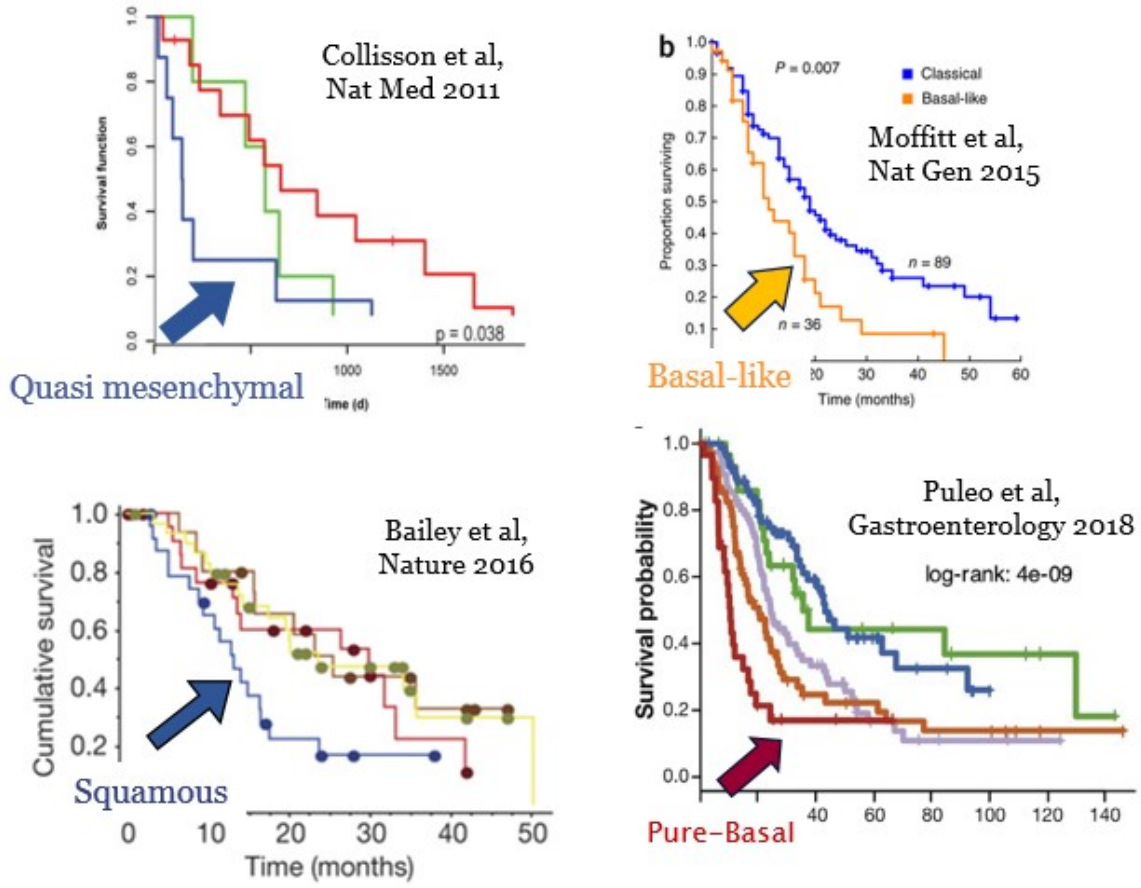

Figure 7: Direct comparison of the different survival probabilities of the published molecular subtypes. Figures retrieved from Collisson et al. (2011), Moffitt et al. (2015), Bailey et al. (2016) and Puleo et al. (2018)[11,52,60,61].

In the first study to differentiate between different PDAC tumor subtypes by Collisson et al., the three subtypes, classical, quasi-mesenchymal and exocrine-like PDAC were defined. This subtyping was initially introduced since survival after tumor resection has been observed to vary based on many factors such as stage and degree of differentiation, however, no factor seemed to be of prognostic value. The quasi-mesenchymal PDAC expressed high levels of mesenchymal genes, while the classical PDAC had a high expression of epithelial and adhesion-associated genes[60]. The exocrine-like subtype mainly expressed digestive enzyme genes but probably represent contaminations from adjacent normal tissue[64]. GATA6 has been associated with the PDAC subtypes and is involved in the development of the pancreas[65–67], while its loss has been linked to the development of PDAC[13,62,68]. In most of the classical subtype samples, GATA6 is overexpressed, while it is relatively low in the quasi-mesenchymal PDAC. Also, by testing the subtype-specific drug responses in cell lines, it was observed that the classical subtype is more sensitive to erlotinib, the inhibitor targeting the tyrosine kinase domain of the epidermal growth factor receptor. Conversely, the quasi-mesenchymal subtype showed

higher sensitivity when treated with gemcitabine. Thus, the two drugs should not be combined when patients are treated since they seem to be effective for distinct groups of patients[60].

The second study on this topic, by Moffitt et al., included also the stromal compartment into their subtyping but defined tumor and stroma subtypes as independent prognostic factors. For this, the samples were digitally microdissected to differentiate between tumor and stromal compartments. Based on the tumor, stroma and normal gene expression, two tumor subtypes, “basal-like” and “classical”, and two stroma subtypes, “normal” and “activated”, were defined. Patients with an activated stroma had a worse prognosis than patients with tumors belonging to the normal stroma subtype, having a shorter median survival time and a lower survival rate. These findings established the hypothesis that interaction between the epithelial and stromal compartments enhance the aggressive nature of PDAC. The basal-like subtype was named after the subtypes of bladder and breast cancer that were defined before, based on a similar gene expression profile, which includes high expression of laminins and keratins[11]. This definition is also interesting since the healthy pancreas consists of simple epithelia and has no basal compartment or any other form of stratified or complex epithelia[69]. Another finding was that the KRAS G12D mutation was mainly observable in the basal-like subtype, while KRAS G12V was identified exclusively in the classical subtype. No differences between the deregulated signaling pathways were associated only with one subtype[11].

In the Bailey et al. study, the tumors were divided into the squamous, pancreatic progenitor, immunogenic and aberrantly differentiated endocrine exocrine (ADEX) subtypes by gene expression analysis. The tumors of the most aggressive subtype, the squamous subtype, harbor TP53, and KDM6A mutations, have an upregulated ΔNp63 transcriptional network and hypermethylated genes involved in the pancreatic endodermal cell fate regulation. In the pancreatic progenitor subtype, high expression of genes involved in the development and cell-fate determination of the pancreas is evident. On the contrary, genes that are essential for the differentiation of the pancreatic progenitor cells into the endocrine or exocrine lineage are overexpressed in the ADEX subtype. Lastly, the immunogenic subtype has been linked to immune infiltrates, showing enrichment of expressed genes that are normally detected in B and T cells. In conclusion, the immunogenic subtype is an innovative subtype from this study, however, the other three subtypes can be grouped together with the subtypes from the two previous studies[52].

These three studies diverge at least to some extent from one another, while also resembling each other. The main reasons for these differences are the methodologies used and the rather small patient’s cohorts. For example, the samples that have been used have been processes differently, Collisson’s samples were microdissected, Moffitt’s were virtually microdissected and Bailey’s were whole tumor samples, selected to have at least 40% of cellularity. Also, the use of different cohorts, technologies, data analysis, and interpretation could already lead to varying results in the same study[63]. However, the basal-like and classical subtypes from the prior study of Moffitt et al. were validated[61]. As the original study already stated, the exocrine-like subtype proposed by Collisson et al. was not represented by PDAC cell lines. Hence, this raised the question if it is an artifact by contamination with normal pancreatic cells, nevertheless, since the samples were microdissected for the enrichment of tumor cells, the study included the subtype into their stratification model[60]. This was already criticized by Moffitt et al. and also in this recent study, the exocrine-like subtype has been again linked to contamination with normal pancreas cells instead of being a subtype of PDAC on its own[61]. In addition, the ADEX and immunogenic subtypes from Bailey et al. have been linked to samples with low purity tumors by the The Cancer Genome Atlas (TCGA) consortium, leaving only the binary classification into the basal-like and classical subtypes[62].

In the most recent study of PDAC subtype stratification by Puleo et al., the tumor and stroma were both taken into consideration, similar to the Moffitt classification. However, these are not handled as independent prognostic factors, leading to a total of five subtypes for the Puleo classification. The PDAC samples were categorized into pure basal-like, stroma activated, desmoplastic, pure classical,

and immune classical. Nevertheless, two classification systems were proposed. The first one focuses only on the neoplastic tumor cells, while the second focuses on the whole tumor as a whole entity. The first classification is in concordance with the Moffitt classification. Though, the second classification of the entire cohort, which has been unsupervised, yielded the five mentioned subtypes. The pure classical subtype is a well-differentiated tumor, while the pure basal subtype is made up of poorly differentiated tumors. The three remaining subtypes, stroma activated, desmoplastic and immune classical, are intermediates on the differentiation scale and also take the stromal compartment around the tumor into account. Mutations in KIT, JAK3, ATM, PTEN, and SMAD4 could not be linked to different subtypes, however, the stroma activated, and pure basal subtypes have been associated with activated MET and GLI1 expression. When comparing the subtypes with each other on the basis of overall survival and disease-free survival, the pure basal PDAC always had the worst prognosis with the shortest overall survival time and short disease-free survival. In contrast to that, the pure classical PDAC had the longest overall survival time and the longest disease-free survival. Stroma activated and desmoplastic subtypes were analyzed more in detail and if the stroma would not have been taken into account, tumors otherwise classified as pure classical or pure basal based on their high tumor cell identification would have identical outlooks. Consequently, this means that high stroma involvement leads to a better prognosis in the case of basal tumors, while at the same time leading to a worse prognosis for classical tumors. In general, the distinction between stroma activated and pure basal can be drawn by the immune infiltrates that are present in the first but not in the second. All these findings, when taken together, underline the importance of the stromal compartment when developing and choosing the right therapy for PDAC[61].

Based on these stratification efforts and their use as prognostic or therapeutic tools, also the hypothesis arose that tumors can be switched between subtypes. This was elaborated, among others, in a study by Adams et al.[70] with a focus on the transcription factor GLI2 and its interference with the Hh signaling pathway. The expression levels of Hh ligands and GLI2 are inversely correlated. GLI2 is overexpressed in basal-like PDAC and leads to a worse prognosis when analyzing RNA-seq data of the TCGA. Overexpression of GLI2 is sufficient to facilitate classical tumors to switch to the basal-like subtype through the activation of mesenchymal genes like VIM, ZEB1 and the basal-like proxy KRT14. The changes were obvious on the protein as well as on the gene expression level, additional to a change towards more elongated and less compact colonies in terms of cell morphology. Furthermore, levels of SHH and GATA6 decreased significantly upon increased expression levels of GLI2 in PDAC cell lines. GLI2 knockdown and knockout experiments were performed with basal-like cell lines, which showed slower tumor growth in tumor xenograft models after transfection. Downstream of GLI2 are various targets, though, the findings highlight the elevated expression of the secreted protein Osteopontin, OPN, that was already linked to several types of cancer. OPN is essential for metastatic growth *in vivo* and helps to establish resistance mechanisms after inhibition of KRAS. Following OPN loss in cells, similar to the loss of GLI2 activity, the KRT14 level decreases and E-cadherin and GATA6 levels increase, seeming to switch into the classical subtype. The data supports that GLI2 is a major transcription factor in the regulation of the basal-like subtype in PDAC and is of importance in PDAC. However, several mechanistic studies need to be conducted since the study mentions GATA6, which based on the results shown, is another anti-correlated marker to GLI2[70]. Interestingly, the less aggressive classical subtype is overexpressing the zinc finger transcription factor GATA6, which also suppresses the SHH pathway, similarly to GLI2; this observation is in agreement with the hypothesis that the encoding gene is a tumor-suppressor gene[11–13,60,71]. In general, when analyzing the expression of GATA6 in the data of the presented subtypes, GATA6 is low across all of the subtypes that have been described as more aggressive and high across the less aggressive subtypes, as depicted in Figure 8.

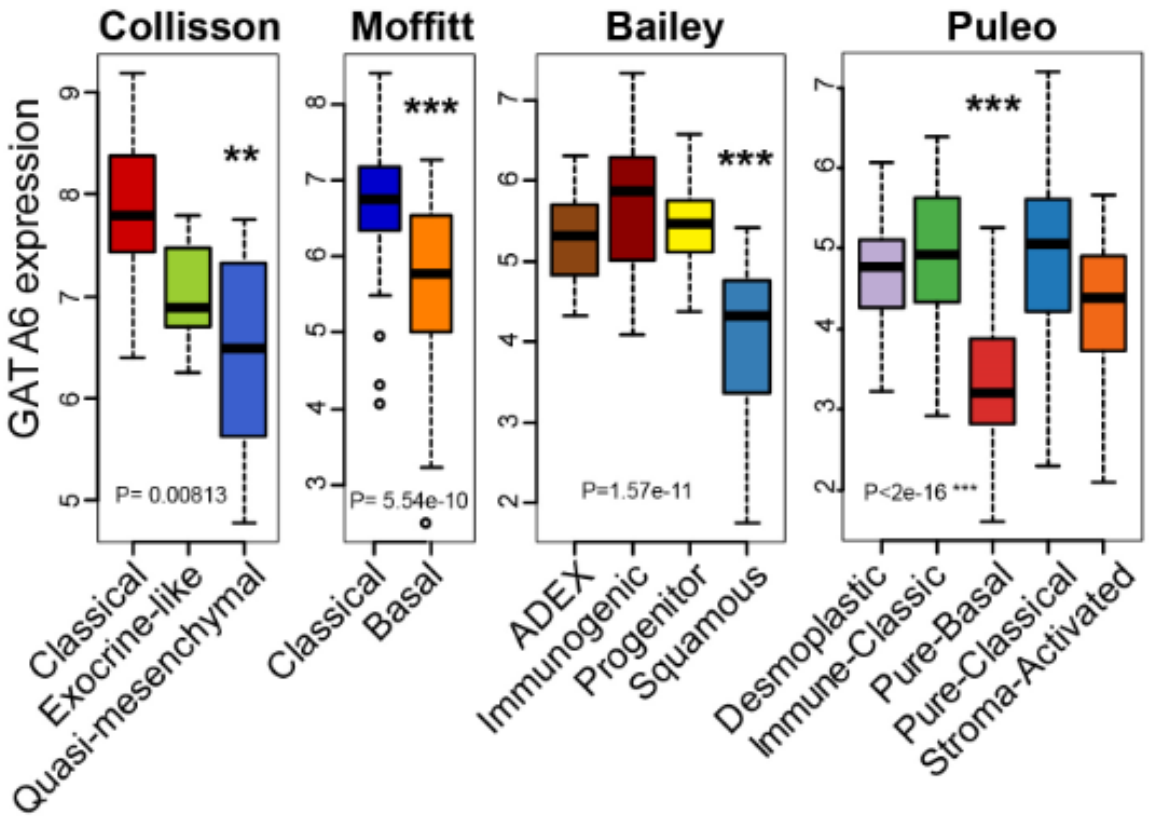

Figure 8: GATA6 is consistently low in the more aggressive phenotype.
Figure retrieved from Kloesch et al., unpublished, manuscript in preparation.

6.4 GATA6

GATA6 is a member of the GATA family of transcription factors. The name stems from the DNA binding motif "GATA" to which the members of this transcription factor family bind[72]. The family is in general involved in numerous developmental processes during embryogenesis and beyond. Additionally, multiple GATA factors have been linked to various human diseases[71]. The zinc-finger transcription factor GATA6 functions as a tumor suppressor gene in pancreatic cancer and plays a crucial role in its development and progression[12]. GATA6 is hypothesized to act as a pioneering transcription factor, which opens the chromatin, as depicted in Figure 9, for numerous other transcription factors, histone modifier and chromatin remodelers in the broader sense. This normally takes place in cooperation with histone acetyltransferases by displacing nucleosomes[73,74].

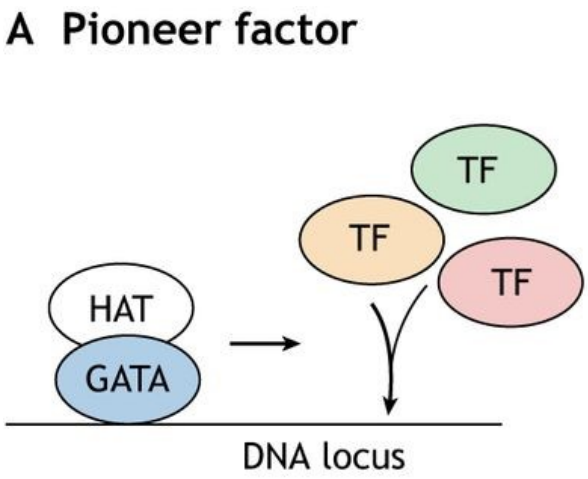

Figure 9: Scheme of GATA6 functioning as a pioneer factor. Figure adapted from Tremblay et al. (2018)[71].

Experiments with mice have shown that when Gata6 is conditionally knocked out after E9.5-10 in addition to the expression of a mutant KRas allele, mice develop tumors earlier than mice with only the KRas aberration. Additionally, mice with just the Gata6 knock out showed no PanINs or tumors, consequently, the loss of Gata6 is not sufficient for tumorigenesis and only acts in cooperation with the KRas activation. Spontaneous loss of Gata6 was observed in several tumors driven by mutant KRas, implying that tumor cells go through a selection process in which the loss of Gata6 is favorable for tumorigenesis. Furthermore, tumors that lost Gata6 show decreased levels of E-cadherin and Krt19, suggesting that the expression of epithelial and differentiation marker is also GATA6-dependent[12]. Based on this and the morphological changes towards the basal-like subtype in cell lines upon GATA6 knockdown, the mechanism of action of the tumor suppression seems to take place via the maintenance of differentiation in epithelial cells and inhibition of EMT. As depicted in Figure 10, the basal keratin KRT14 was detectable only in tumor regions with low GATA6 levels, while it could not be detected in regions with high levels of GATA6. As previously mentioned, patients with a tumor that expresses high levels of GATA6 have a better survival prognosis and are normally classified under the classical subtype. Through these mechanisms, the involvement of GATA6 in the inhibition of the development of the tumor, as well as the progression towards metastasis, was confirmed both directly through the regulation of epithelial and mesenchymal genes and indirectly via the regulation of transcription factors that act pro-epithelial or pro-mesenchymal[13].

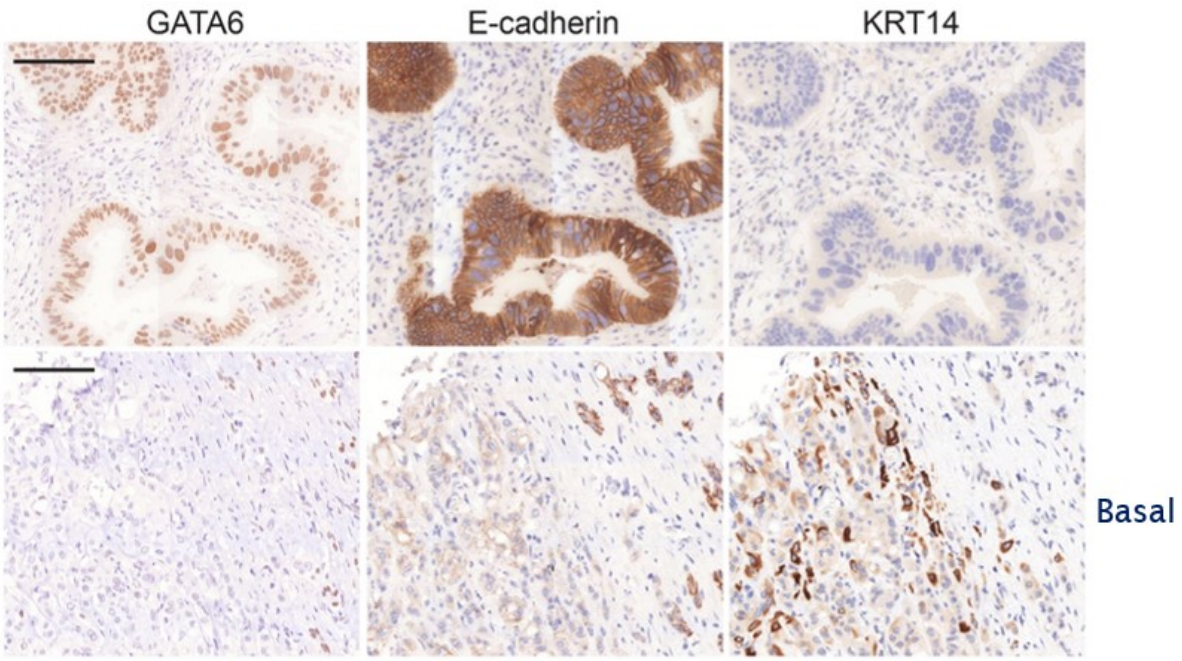

Figure 10: GATA6 regulates EMT and is associated with an altered phenotype. Figure adapted from Martinelli et al. (2016)[13].

To study this more in detail, it was pivotal that the mouse model is comparable to the situation in humans. Therefore, different mouse models were compared to human patient samples. Mice with wildtype Gata6 show spontaneous loss to the same extent as patients, as illustrated in Figure 11. In addition, it was also observed that heterozygous animals are more inclined to lose Gata6 and that all mice in which Gata6 was knocked out only after around 4 months, had undetectable levels of GATA6 in the samples, meaning that the late KO model is effective. The late KO model was introduced since GATA6 is essential in embryonic development and mice with non-conditional total knockouts die 5.5 to 7.5 days post coitum due to defects in the function of the visceral endoderm[75,76]. Additionally, a late KO reflects the tumorigenesis of PDAC more closely, since PanINs express GATA6 and then only after they developed into tumors GATA6^{neg} regions can be found.

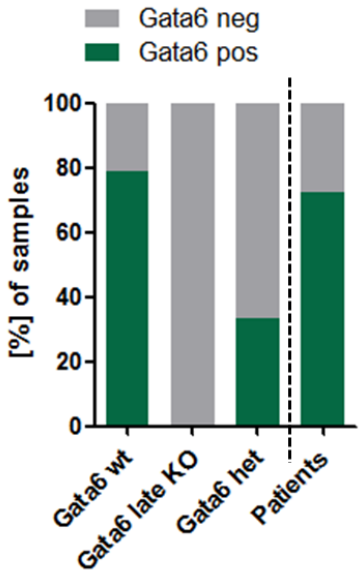

Figure 11: Gata6 is lost in humans and mice spontaneously to the same extent.
Figure adapted from Kloesch et al., unpublished, manuscript in preparation.

Associated with the GATA6 expression levels is the expression of KRT14, as already shown in Figure 10. KRT14 is only detectable when GATA6 is lost, demonstrating a negative correlation. To assess if the

loss of GATA6 is necessary for KRT14 to be expressed mice samples were used. Strikingly, as illustrated in Figure 12A, mice harboring wildtype GATA6 show KRT14 positive regions. However, upon further analysis, all KRT14 positive regions could be linked to mice which lost GATA6 spontaneously. Since the GATA6 status of humans and mice were similar, also the distribution of KRT14 positive and negative regions according to the genotype were in concordance to each other. In conclusion, the loss of GATA6 expression is necessary for ectopic expression of KRT14 in mouse and human and, more in general, for the emergence of the basal-like phenotype in PDAC.

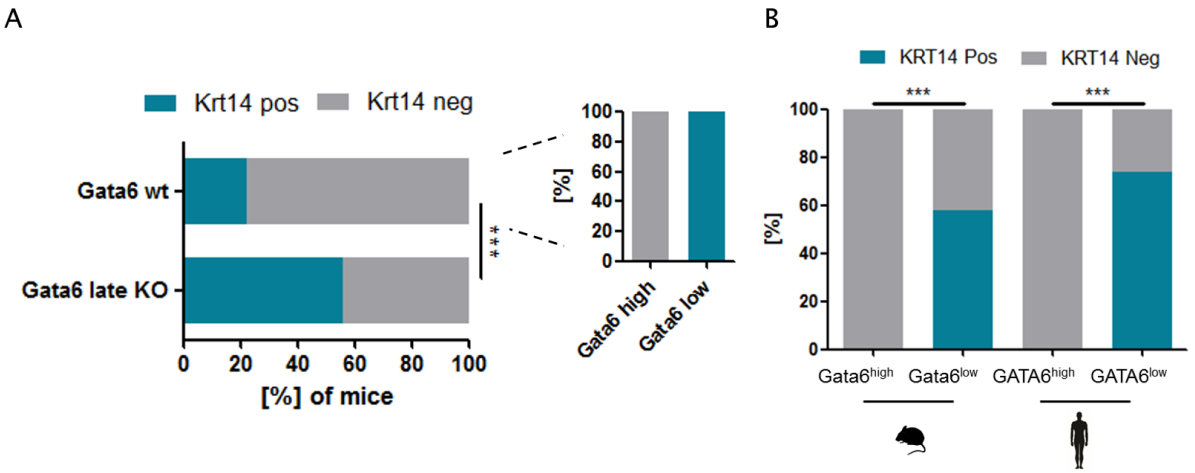

Figure 12: Loss of GATA6 expression is necessary for the ectopic expression of KRT14 in mice and humans. Figure adapted from Kloesch et al., unpublished, manuscript in preparation.

Indeed, GATA6 has increased transcriptional activity during the shift from the basal-like to the classical phenotype[77]. Therefore, the contribution of GATA6 needs to be further clarified to improve the treatment options of PDAC.

6.5 ΔNp63 & Epigenetics

When sequencing the exome of eight PDAC patients who survived longer than 10 years to investigate if very long-term survivors of PDAC have specific genetic alterations, no difference in the commonly mutated genes was observed[78]. This supports that epigenetic events generate the observed heterogeneity and decode shared charecteristics[53,54,77,79].

Additional evidence demonstrates that squamous tumors harbor an increased number of mutations in TP53 and KDM6A, upregulation of the transcriptional network around ΔNp63, as well as hypermethylation of pancreatic developmental genes like GATA6[52]. The loss of the histone demethylase KDM6A, located on the X chromosome, is not only observable in the squamous subtype, but the subtype can be specifically induced through the ablation of KDM6A in females, which supports the connection and confirms that KDM6A loss is sufficient to induce squamous PDAC in women. For this subtype to develop in males the Y chromosome-encoded histone demethylase paralog UTY had to be lost in addition. These losses are in association with the upregulation of ΔNp63 expression and are associated with a shorter life expectancy[53]. Different mechanisms were proposed for the tumor-promoting activity of ΔNp63, one of them by antagonizing p53[80], however, ΔNp63 is necessary and sufficient for the enhancer reprogramming towards the squamous subtype. This change in the enhancer landscape results in the promotion of de-differentiation, invasion, and migration[54]. These biological programs are in concordance to ΔNp63's role in squamous epithelial tissues and cell carcinomas[81].

Superenhancers (SEs) are clusters of enhancers that have the histone mark H3K27ac and control the transcription of genes that are involved in differentiation and other developmental processes[53]. H3K27ac is used to identify active promoters and enhancers, therefore, this histone mark can be used as a proxy for activated gene transcription[55]. The loss of KDM6A in mice did not show a significant increase in H3K27me3 in the SEs indicating that this specific mechanism is not methylase activity-dependent. The female knockout mice activated gene networks around p63, ZEB1, RUNX3 and MYC, which all drive the squamous subtype and metastasis. Additionally, it has been found that tumors with low levels of KDM6A are selectively sensitive to BET inhibitors by showing a reduction in proliferating cells[53]. Upon knocking down ΔNp63 in squamous PDAC cell lines, a decrease in the proliferative potential was observed. All in all, this leads to the insight that the cell programming and the molecular subtypes are closely linked to various master transcription factors, which are interconnected with superenhancers and downstream pathways, and regulate each other[55].

Several studies show that the squamous subtype is caused by ΔNp63 and subsequent changes in the epigenetic reprograming[53–55]. Unfortunately, no connection between the ΔNp63/squamous subtype and GATA6/classical subtype relationships could have been drawn yet. Unpublished data from the manuscript by Kloesch et al. shows in Figure 13A, that an inverse correlation of TP63 and GATA6 was observed in two patient cohorts. For this data analysis, the datasets of the studies of Bailey et al.[52] and Puleo et al.[61] were used. The data uses TP63, which would be both the long isoform TAp63 and the short ΔNp63, however, pancreatic cell lines, which harbor p53 mutations, as most PDAC cell lines do, do not express or express TAp63 in a decreased manner. p53 appears to inhibit TAp63 through mechanisms that are currently still unknown[82]. Consequently, this supports that the depicted TP63 in Figure 13A is mainly ΔNp63. In addition to that, a Gene Set Enrichment Analysis (GSEA) of the dataset from the Bailey study and the available data of The Cancer Genome Atlas, show an upregulation of ΔNp63 target in GATA6 low tumors as depicted in Figure 13B.

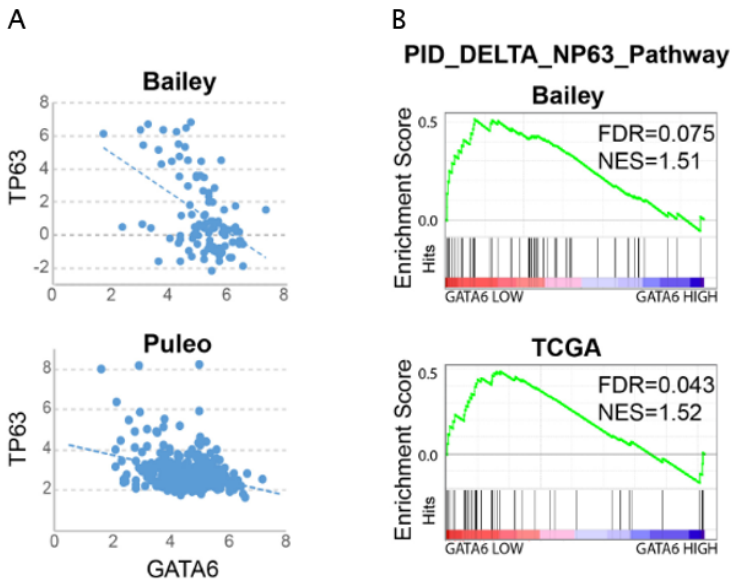

Figure 13: Upregulation of ΔNp63 targets is observed in GATA6 low tumors.
Figure adapted from Kloesch et al., unpublished, manuscript in preparation.

When performing immunohistochemistry on patient samples, the negative correlation of TP63 and GATA6 was confirmed. Regions of tumors with GATA6 expression show no expression of p63, whereas in regions with p63, GATA6 is not detectable. Consequently, the loss of GATA6 expression is necessary for the upregulation of TP63, and also the ectopic expression of KRT14, which was already mentioned in 6.3 Molecular subtypes. Based on this correlation with each other, KRT14 has also been used as a proxy for TP63 expression in this study. The quantifications of the immunohistochemistry finally showed a statistically significant difference in p63 expression between tumors expressing GATA6 in low or high levels. Interestingly, ten tumors of the GATA6^{high} category showed focal p63 expression, however, after careful revision, it became clear that the foci of p63 expression were always GATA6-negative. Only one tumor has a p63-GATA6 double-positive small focus, which needs to be further confirmed with independent analysis.

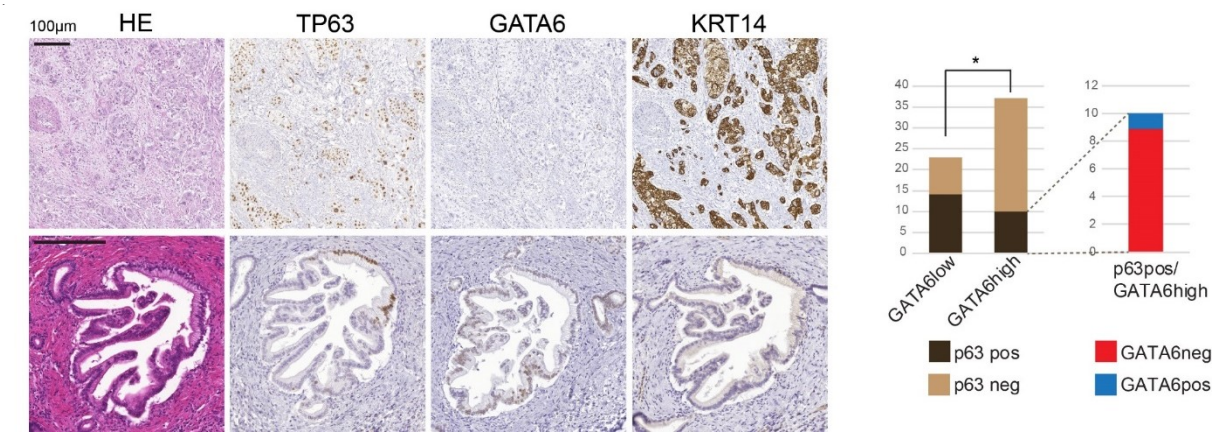

Figure 14: Loss of GATA6 expression is necessary for the upregulation of TP63 and ectopic expression of KRT14.
Figure adapted from Kloesch et al., unpublished, manuscript in preparation.

7 Aims and scope

This project has the aim of studying the possible role of GATA6 in regulating the epigenetic changes in PDAC and of analyzing whether GATA6 inhibits the ΔNp63-driven basal phenotype in PDAC.

To address these questions, our first aim was to generate GATA6 overexpressing and GATA6 knockdown human PDAC cell lines using lentiviral transduction. Overexpression was performed with two basal-like established cell lines, namely BxPC-3 and L3.6pl, and knockdown of GATA6 was performed with the classical phenotypical cell line PaTu8988S. These cell lines would then serve as research tools by allowing the exploration of GATA6 effects on the molecular mechanisms driving the basal-like phenotype. In the next step, it was aimed to characterize these cell lines for the expression of GATA6 and various markers that could be affected, either directly or indirectly, on a protein and gene expression level. In addition, we planned to assess changes in the chromatin by chromatin immunoprecipitation in response to overexpression or knockdown of GATA6. Another important aim was to evaluate the proliferation, migration, and invasion of the cell lines after gain- or loss-of-function of this crucial transcription factor. However, this was only conducted for the cell line BxPC-3 since the lab already published functional assay data on the other two cell lines which were used during this project.

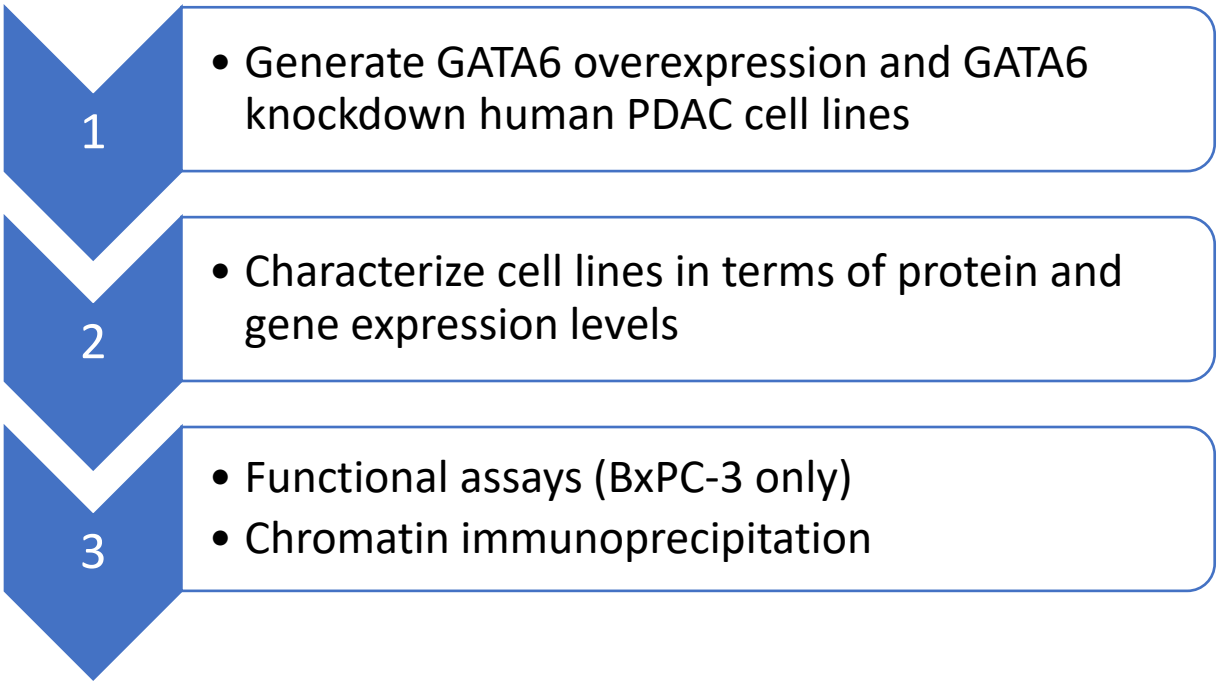

Figure 15: Scheme of the project's workflow.

The aim of this project is to study the involvement of GATA6 in the subtypes of PDAC, especially if the overexpression of GATA6 is sufficient to shift the cancer into the less aggressive phenotype. Based on this knowledge, better personalized therapy based on the subtypes of PDAC and also more efficient therapy in general for this lethal cancer could be developed.

8 Results

8.1 Effects of GATA6 overexpression in the human PDAC cell line BxPC-3

8.1.1 Characterization of GATA6 overexpression effects on protein expression in BXPC3 cells

Stable cell lines were generated by lentiviral transduction of the BXPC3 cell line. The cells were expanded and subsequently sorted for GFP-positive cells. To assess if the overexpression of GATA6 alters the protein expression in BXPC3 cells, Western Blot has been performed. The protein expression was examined with anti-GATA6, anti-p63, anti-KRT14, anti-Vinculin, anti-E-cadherin, and anti-GAPDH-antibodies. GATA6 expression levels were visibly higher, confirming the successful overexpression at the protein level. Also, E-cadherin levels were modestly increased, as previously reported in L3.6pl cells[13]. In contrast, the protein levels of ΔNp63 and KRT14 were lower in GATA6-overexpressing cells (Figure 16A). The indicated ΔNp63 was detected at a size of 65kDa and corresponds to ΔNp63α, the second isoform of p63[83]. All changes were statistically significant as represented in the bar chart in Figure 16B.

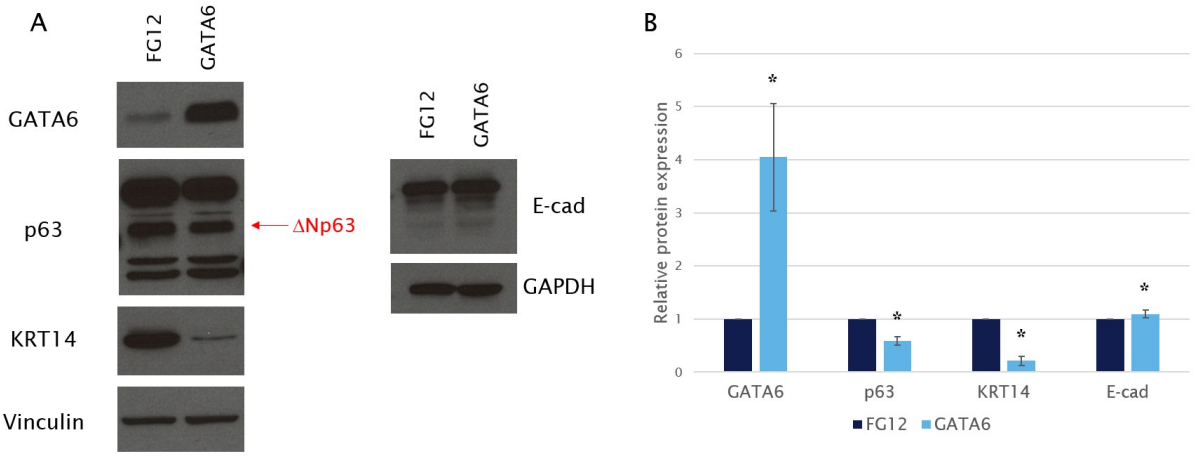

Figure 16: GATA6 overexpression leads to the downregulation of DNp63 and KRT14 on the protein level. *[A] BXPC3 cells stably expressing empty vector (=FG12) or GATA6 were analyzed for the expression of GATA6, p63, KRT14 and E-cadherin using Western Blot. Vinculin and GAPDH loading controls are indicated. [B] GATA6, p63, KRT14, and E-cadherin bands were quantified using ImageJ 1.52p software, normalized according to the loading controls, the protein expression ratio relative to FG12 was calculated and visualized using a chart diagram. Error bars represent the standard deviation of four independent experiments. Statistical analysis was performed using a two-tailed Student's t-test. *, p<0.05.*

8.1.2 Characterization of GATA6 overexpression effects on gene expression in BXPC3 cells

At the same time as BXPC3 cells were seeded and processed for Western Blot analysis, cells were also seeded and processed for quantitative reverse transcription followed by PCR (RT-qPCR) to analyze if the overexpression of GATA6 alters the gene expression in BXPC3 cells. The expression levels were examined for several genes connected to the classical or basal subtype; and in addition, some mesenchymal genes were also measured. GATA6 overexpression was detectable on the gene expression level, confirming the overexpression (Figure 17). In general, classical genes (dark blue) showed an increase in gene expression, while the basal-like gene (orange) expression decreased. The downregulation of KRT14 and the two isoforms of p63, TAp63 (long isoform) and ΔNp63 (short isoform); and the upregulation of CDH1 (=E-cadherin) were confirmed on the RNA level, supporting the results of the Western Blot analysis in Figure 16. Additional significant downregulations were found in KRT5, FAT2, and S100A2, while FOXA1 was found to be upregulated significantly. Interestingly, several mesenchymal genes (purple) including N-cadherin (CDH2), SNAI1, SNAI2, VIM, and TWIST1 were moderately upregulated, although the changes were statistically significant only for CDH2 (Figure 17). This could be hinting that the basal phenotype and the EMT are not necessarily linked to each other.

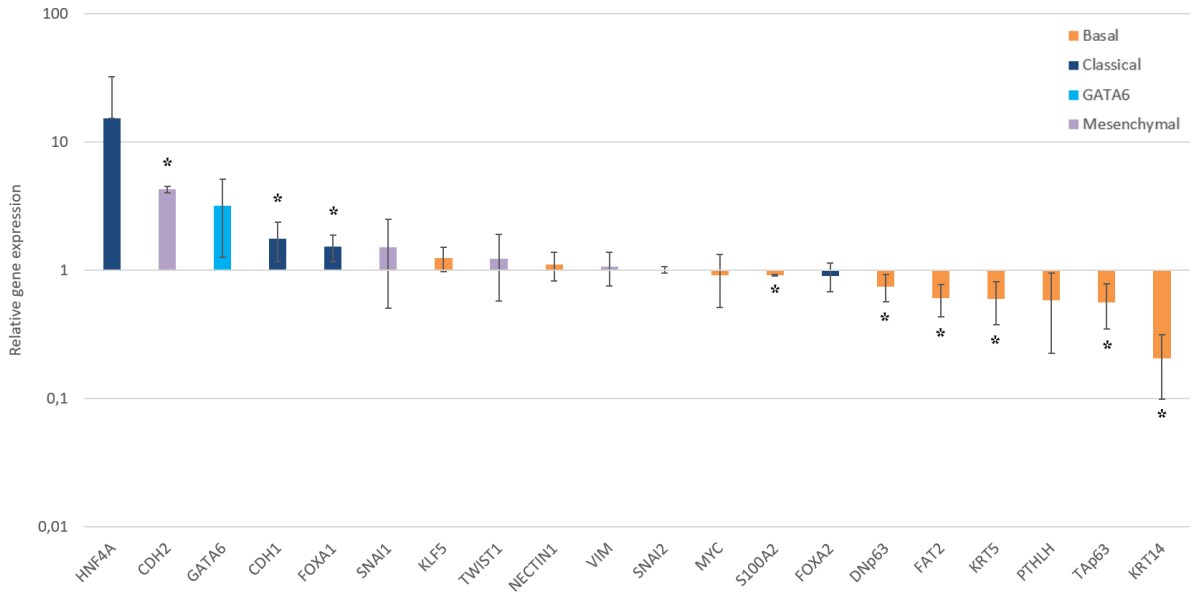

Figure 17: GATA6 overexpression leads to the downregulation of genes that are associated with the basal-like phenotype. *Differences in the gene expression levels of the indicated genes were analyzed in BXPC3 cells stably expressing empty vector (=FG12) and GATA using quantitative reverse transcriptase PCR. Gene expression levels were obtained as Ct values, normalized according to HPRT control, the relative to FG12 gene expression ratio was calculated and visualized using a chart diagram. Error bars represent the standard deviation of four independent experiments. Statistical analysis was performed using a two-tailed Student's t-test. *, p<0.05.*

8.1.3 Functional assays

8.1.3.1 Proliferation assays of BXPC3 cells stably expressing GATA6 compared to empty vector

To investigate if the overexpression of GATA6 alters the proliferation in BXPC3 cells, proliferation assays have been conducted. The empty vector-transduced cells and the GATA6 overexpressing cells were compared in two growth curve experiments (Figure 18A) as well as in one Bromodeoxyuridine (BrdU) assay (Figure 18B). In the growth curve experiments, the GATA6 overexpressing cells had a higher cell count until day 4, however, the cell number dropped slightly on day 5 of the experiments. Due to high variability, no significant difference for the proliferation was observable. With the BrdU assay, the proliferation rate was analyzed. This is based on the amount of BrdU that is incorporated into the nuclei during a given time window. The BrdU-positive nuclei in the resulting pictures were counted and the proliferation rate was calculated. The values of FG12 and GATA6 BXPC3 cells are almost identical. Both assays show high standard deviations, therefore, no statistically significant change in the proliferative potential was observed in GATA6 overexpressing BXPC3 cells when compared to the empty vector.

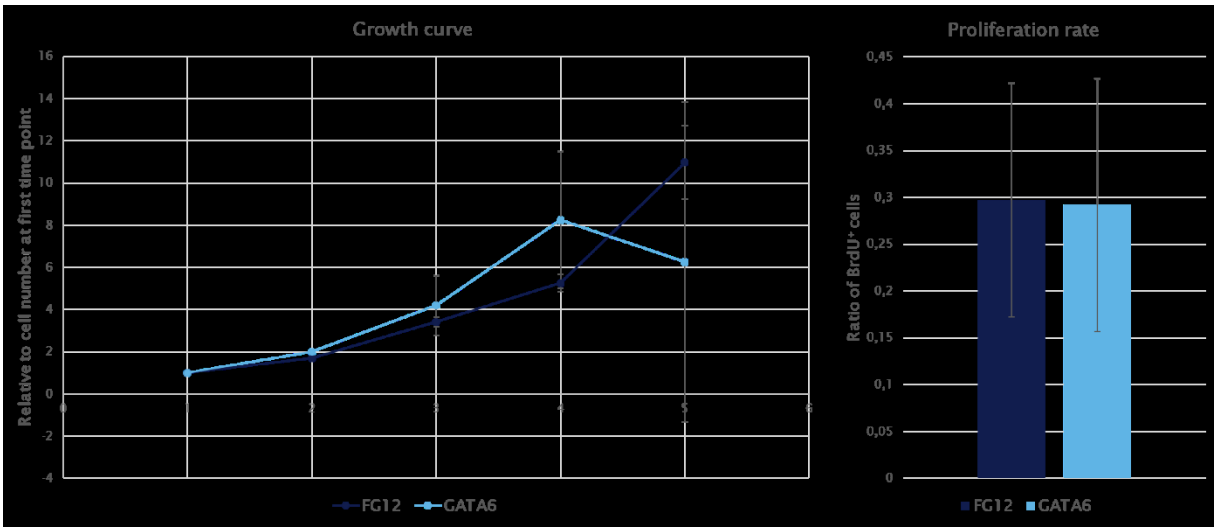

Figure 18: Proliferation is not affected by GATA6 overexpression. *Cells were cultured as normal and seeded for growth curve (A) and Bromodeoxyuridine (BrdU) assays (B). [A] The cell counts are shown as relatives to the counted cell number at the first time point. The error bars represent the standard deviation of two independent experiments. [B] The cells in the BrdU assay were treated with BrdU for 2 hours prior to fixation and stained with anti-BrdU antibody. The error bars represent the standard deviation of the nuclei counts between the acquired pictures. Statistical analysis was performed using a two-tailed Student's t-test. *, p<0.05.*

8.1.3.2 Migration assays of BXPC3 cells stably expressing GATA6 compared to empty vector

To investigate if the overexpression of GATA6 alters the migratory potential in BXPC3 cells, wound healing assays have been conducted. Empty vector-transduced and GATA6-overexpressing cells were compared to each other in three replicate experiments. A tendency towards slower migration of GATA6-overexpressing cells was observed 24h and 48h after the scratch. However, due to the variation between three independent experiments, no significant difference was detectable (Figure 19).

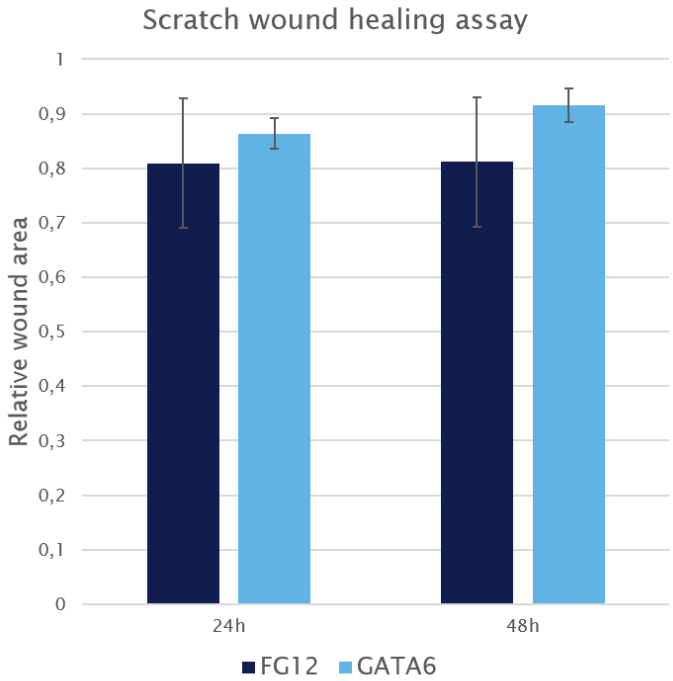

Figure 19: GATA6 overexpression does not alter BXPC3's ability to migrate in vitro. *Graph showing the relative wound area 24h and 48h after scratching in control and GATA6-overexpressing cells. The error bars represent the standard deviation of three independent experiments. Statistical analysis was performed using a two-tailed Student's t-test. *, p<0.05.*

8.1.3.3 Invasion assays of BXPC3 cells stably expressing GATA6 compared to empty vector

To investigate if the overexpression of GATA6 alters the ability of BXPC3 cells to invade into the extracellular matrix, Transwell Matrigel invasion assays have been conducted. The values were normalized according to the invaded cell number of FG12-transduced cells after 24 hours. During the first 24 hours, GATA6 overexpressing cells were invading the membrane faster than the control. Nevertheless, after 48 hours the FG12-transduced cells surpassed the invasive potential of the GATA6 overexpressing cells slightly. Still, due to the variation between three independent experiments, the detected differences were not statistically significant (Figure 20).

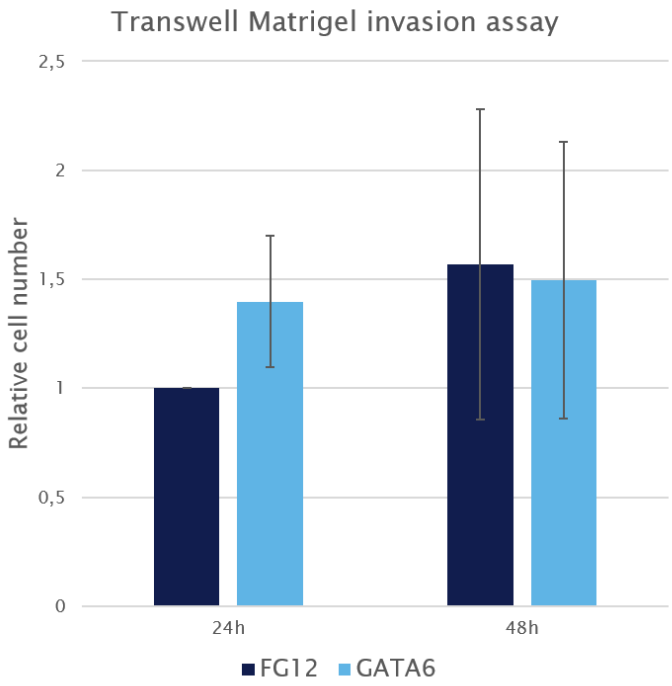

***Figure 20: GATA6 overexpression does not alter BXPC3's ability to invade in vitro**. Relative cell numbers of Matrigel invasive cells are shown after 24 and 48 hours. The cell number per area was calculated and subsequently normalized according to the invaded cell number of FG12 cells after 24 hours in culture. The error bars represent the standard deviation of three independent experiments. Statistical analysis was performed using a two-tailed Student's t-test. *, p<0.05.*

8.1.4 Characterization of GATA6 overexpression effects on the chromatin in BXPC3 cells

8.1.4.1 Chromatin immunoprecipitation of the histone mark H3K27ac

Cells were seeded and processed for chromatin immunoprecipitation (ChIP) with successive qPCR to analyze if the overexpression of GATA6 alters the chromatin landscape in BXPC3 cells. The chromatin occupation levels of the histone mark H3K27ac were examined for the promoters of several genes connected to the classical or basal subtype and also of *GATA6* and negative control. GATA6 overexpression led to an increase of the histone mark H3K27ac, which marks transcriptional active genes, around the transcription start site of GATA6 itself. Nevertheless, the increase in the "classical" gene HNF4A (dark blue), as well as in several basal-like genes (orange) points to the concept that GATA6 overexpression increases the levels of H3K27ac histone marks on the chromatin but is not gene-specific. Interestingly, the overexpression of GATA6 also caused an increase in H3K27ac on the negative control (red), which was chosen since it was found in a gene desert, a region of the genome that is free of genes and therefore, not coding for proteins. This shows that all in all, the overexpression led to a general increase in the acetylation of histone 3 on lysine 27 throughout the analyzed gene panel and, therefore, the opening of the chromatin appears to be of a non-gene-specific manner (Figure 21).

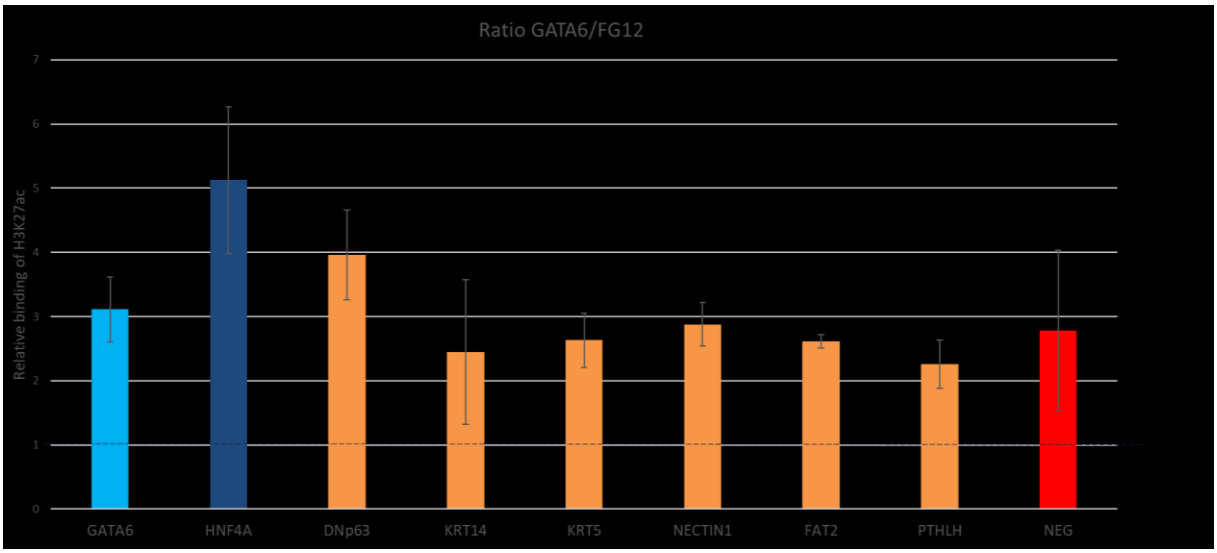

Figure 21: Chromatin seems to be generally more open when GATA6 is overexpressed. *Stably expressing empty vector (=FG12) and GATA6 BXPC3 cells were untreated and subsequently used for chromatin immunoprecipitation. Differences in the chromatin pulldown of H3K27ac in the indicated genes were detected using quantitative PCR. H3K27ac chromatin occupation levels were obtained as Ct values, normalized according to the relative of FG12 chromatin occupation levels and visualized using a chart diagram. The error bars represent the standard deviation of three independent experiments. Statistical analysis was performed using a two-tailed Student's t-test. *, p<0.05.*

8.1.4.2 Chromatin immunoprecipitation of the transcription factor GATA6

The chromatin occupation levels of GATA6 itself were examined in the same regions analyzed for H3K27ac. GATA6 overexpression led to an increase of GATA6 binding to its own promoter (light blue). This is consistent with previous ChIP and ChIP-Seq data showing that GATA6 binds to its own promoter[13]. As for the H3K27ac ChIP (Figure 21), the highest peak is on the promoter of the classical gene HNF4A (dark blue), suggesting that GATA6 leads to the transcriptional activation of HNF4A through the binding of the promoter and its opening, based on the H3K27ac readout. In general, the basal-like genes (orange) only show a moderate increase in GATA6 promoter occupation, suggesting that GATA6 does not have a major direct regulation of their transcription. The binding of GATA6 to the promoter of ΔNp63 does not increase significantly and the binding on KRT5 and KRT14, which have been found to be downregulated in the RT-qPCR analysis (Figure 17), also show only a slight increase in GATA6 occupancy. Again, the negative control shows a slightly higher binding of the protein that was pulled down and no strong gene-specificity could be observed (Figure 22). In general, the biological replicates showed a rather high variability, and none of the mentioned enrichment reached statistical significance.

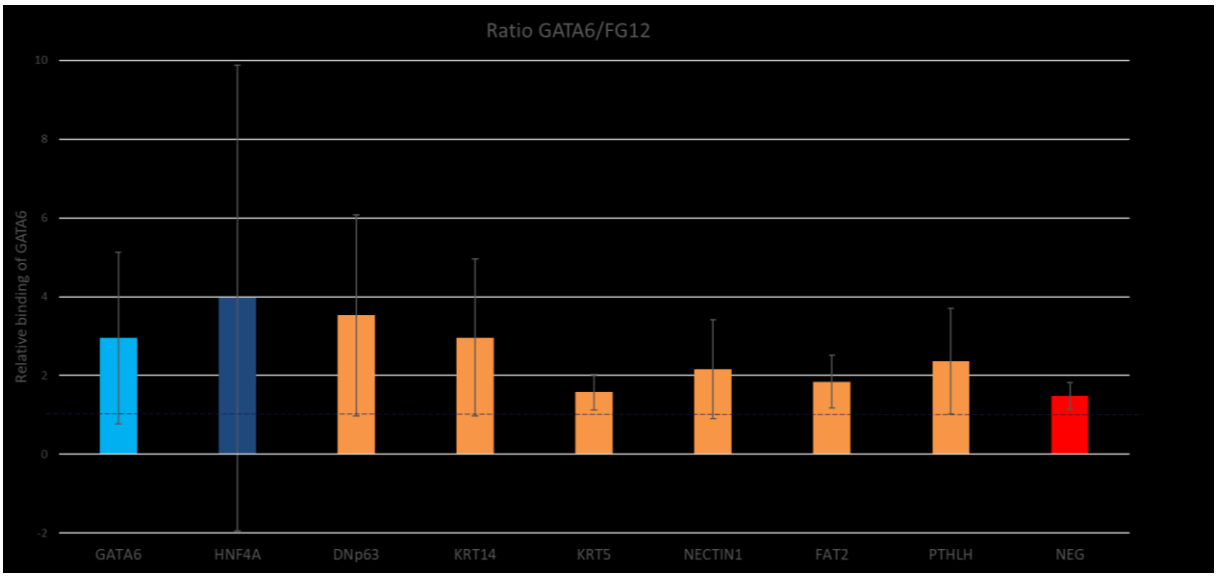

Figure 22: GATA6 seems to have direct and indirect activity. *Stably expressing empty vector (=FG12) and GATA6 BXPC3 cells were untreated and subsequently used for chromatin immunoprecipitation. Differences in the chromatin pulldown of GATA6 in the indicated genes were detected using quantitative PCR. GATA6 chromatin occupation levels were obtained as Ct values, normalized according to the relative of FG12 chromatin occupation levels and visualized using a chart diagram. The error bars represent the standard deviation of four independent experiments. Statistical analysis was performed using a two-tailed Student's t-test. *, p<0.05.*

8.2 Effects of GATA6 overexpression in the human PDAC cell line L3.6pl

8.2.1 Characterization of GATA6 overexpression effects on protein expression in L3.6 cells

Western Blot has been performed to assess which effect the overexpression of GATA6 has on the expression of basal-related proteins in L3.6 cells. With anti-GATA6, anti-p63, anti-KRT14, anti-Vinculin, anti-E-cadherin, and anti-GAPDH-antibodies the protein expression was examined. The successful introduction of the overexpression was confirmed by visibly higher GATA6 expression on the protein level. The E-cadherin levels were slightly increased as well, while KRT14 levels were slightly decreased. In contrast to the BXPC3 cells, the protein levels of p63 were higher upon GATA6 overexpression (Figure 23A). The changes were not of statistical significance as depicted in Figure 23B.

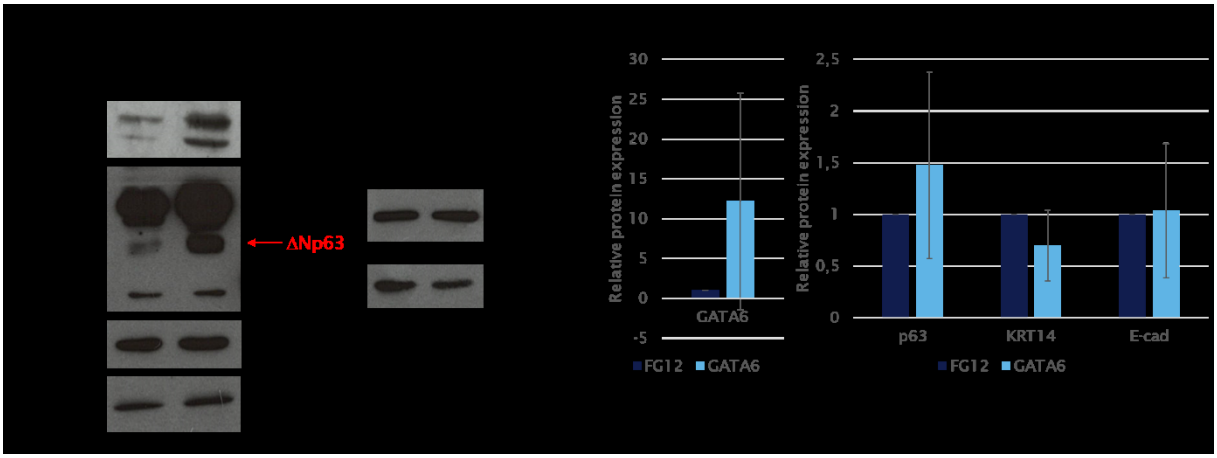

Figure 23: GATA6 overexpression in L3.6 shows an opposite effect when compared with BXPC3. *[A] L3.6 cells stably expressing empty vector (=FG12) or GATA6 were analyzed for the expression of GATA6, p63, KRT14 and E-cadherin using Western Blot. Vinculin and GAPDH loading controls are indicated. [B] GATA6, p63, KRT14, and E-cadherin bands were quantified using ImageJ 1.52p software, normalized according to the loading controls, the protein expression ratio relative to FG12 was calculated and visualized using a chart diagram. Error bars represent the standard deviation of three independent experiments. Statistical analysis was performed using a two-tailed Student's t-test. *, p<0.05.*

8.2.2 Characterization of GATA6 overexpression effects on gene expression in L3.6 cells

As previously described in the chapter 8.1.2, also L3.6 cells were processed for RT-qPCR. This was conducted to evaluate how the GATA6 overexpression changes the gene expression profile. The overexpression was confirmed on the gene expression level and classical genes (dark blue), as well as basal-like genes (orange), showed an increase in expression. This led to a different signature in comparison to the protein data (Figure 23) and the BXPC3 cell line (Figure 17). Only the expression of PTHLH seemed to be downregulated, however, this change is not of statistical significance. The only genes, which show a statistically significant change are FOXA2 and FAT2, which are upregulated. For these samples, no additional mesenchymal genes were analyzed since the upregulation of N-cadherin (CDH2) was not observable in each of the four experiments and therefore, is not of statistical significance (Figure 24). In addition, the mesenchymal genes from our panel have already been analyzed in the previously mentioned study for the L3.6 cells[13].

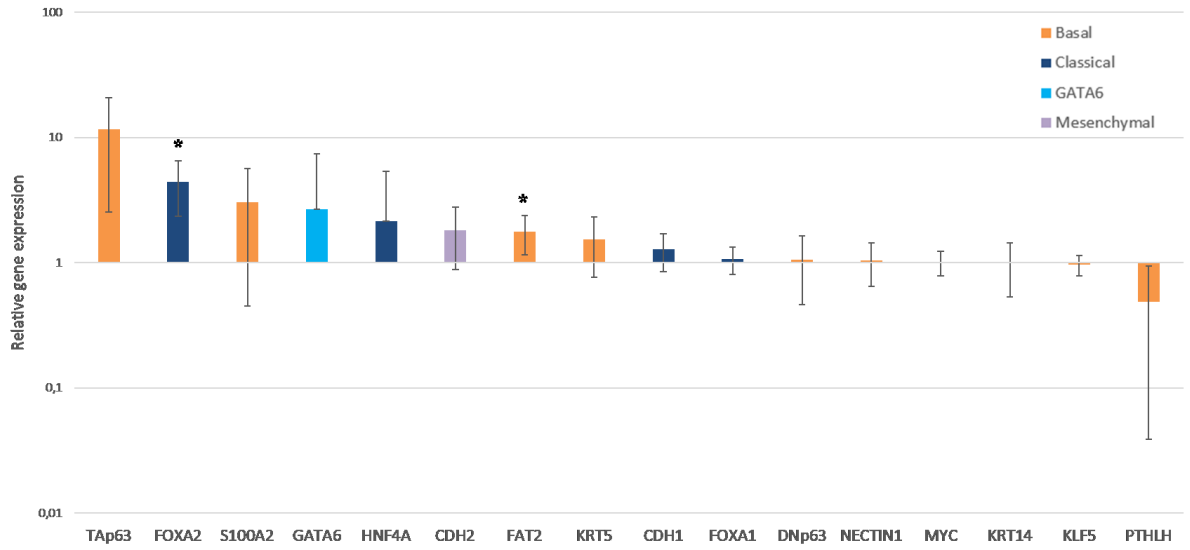

Figure 24: GATA6 overexpression leads to different gene expression signatures when compared to BXPC3 & L3.6 protein expression. *Differences in the gene expression levels of the indicated genes were analyzed in L3.6 cells stably expressing empty vector (=FG12) and GATA using quantitative reverse transcriptase PCR. Gene expression levels were obtained as Ct values, normalized according to HPRT control, the relative to FG12 gene expression ratio was calculated and visualized using a chart diagram. Error bars represent the standard deviation of four independent experiments. Statistical analysis was performed using a two-tailed Student's t-test. *, p<0.05.*

8.2.3 Characterization of GATA6 overexpression effects on the chromatin in L3.6 cells

8.2.3.1 Chromatin immunoprecipitation of the histone mark H3K27ac

The openness of the chromatin was assessed in L3.6 cells by ChIP-qPCR (chromatin immunoprecipitation with successive qPCR). The abundance of the histone mark H3K27ac was analyzed across a few genes connected to the basal subtype and in addition, also to GATA6 and negative control. In general, the histone mark is indicating transcriptional active genes and therefore, suggests an increase of GATA6 expression based on the H3K27ac marks around the transcription start site of GATA6 itself, which validates our GATA6 overexpression model now also on the chromatin level. The basal-like genes(orange), ΔNp63, TAp63 and KRT14, show increases in their levels of H3K27ac histone marks on the chromatin upon GATA6 overexpression. Again, the increase in H3K27ac on the negative control (red) is observable, suggesting the lack of gene-specificity across cell lines. Overall, the overexpression leads to a generally more open chromatin (Figure 25).

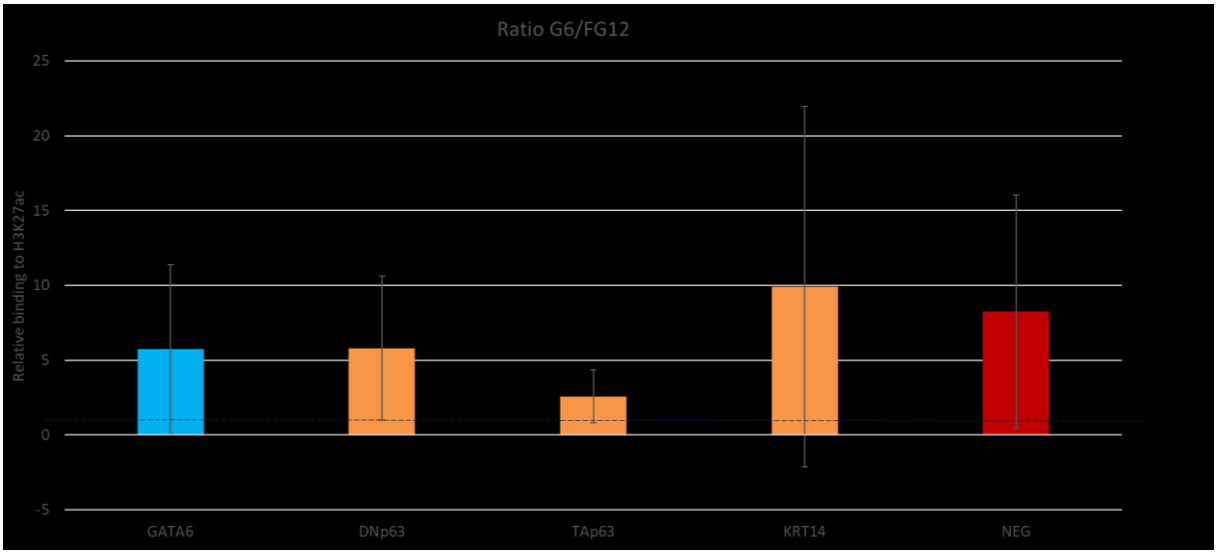

Figure 25: Chromatin seems to be generally more open when GATA6 is overexpressed. *Stably expressing empty vector (=FG12) and GATA6 L3.6 cells were untreated and subsequently used for chromatin immunoprecipitation. Differences in the*

*chromatin pulldown of H3K27ac in the indicated genes were detected using quantitative PCR. H3K27ac chromatin occupation levels were obtained as Ct values, normalized according to the relative of FG12 chromatin occupation levels and visualized using a chart diagram. The error bars represent the standard deviation of three independent experiments. Statistical analysis was performed using a two-tailed Student's t-test. *, p<0.05.*

8.2.3.2 Chromatin immunoprecipitation of the transcription factor GATA6

A few genes connected to the basal subtype, GATA6, and negative control were evaluated via ChIP-qPCR to detect alterations in GATA6 occupancy in response to GATA6 overexpression. GATA6 overexpression led to an increase of GATA6 occupying its own promoter (light blue). Out of the basal-like genes (orange), ΔNp63 seems to be the only one targeted directly by GATA6. TAp63 and KRT14 suggest indirect targeting through ΔNp63. Once more, the negative control shows higher binding of the protein, that was pulled down, and for the high variance between the three independent experiments, no statistically significant changes could be observed (Figure 22).

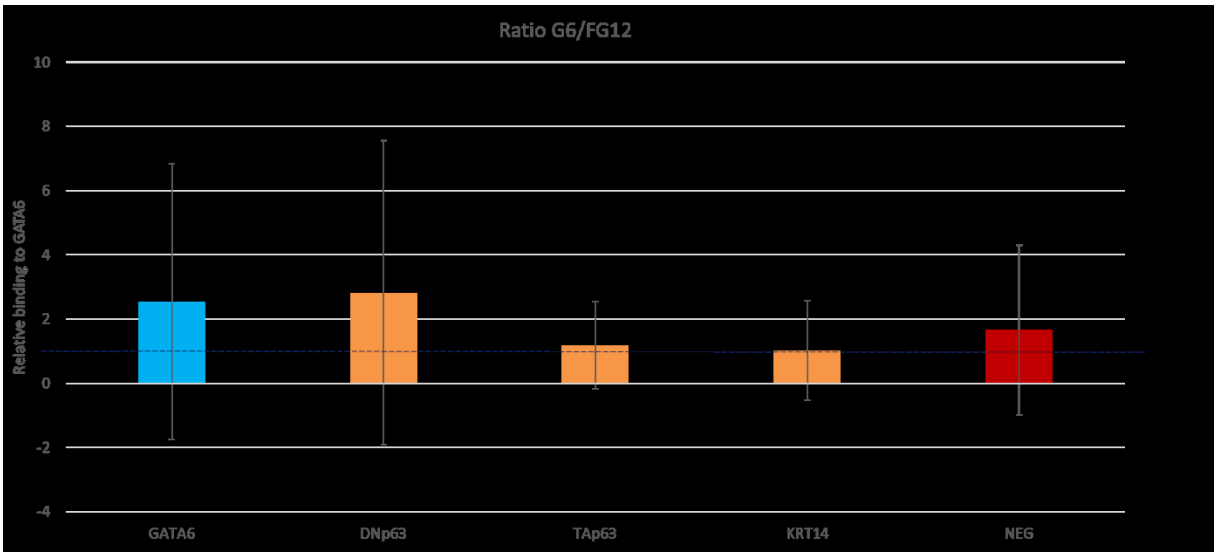

Figure 26: ΔNp63 seems to be directly targeted by GATA6. *Stably expressing empty vector (=FG12) and GATA6 L3.6 cells were untreated and subsequently used for chromatin immunoprecipitation. Differences in the chromatin pulldown of GATA6 in the indicated genes were detected using quantitative PCR. GATA6 chromatin occupation levels were obtained as Ct values, normalized according to the relative of FG12 chromatin occupation levels and visualized using a chart diagram. The error bars represent the standard deviation of three independent experiments. Statistical analysis was performed using a two-tailed Student's t-test. *, p<0.05.*

8.3 Effects of GATA6 knockdown in the human PDAC cell line PaTu8988S

8.3.1 Characterization of GATA6 knockdown effects on protein expression in PaTu cells

Stable cell lines were generated by lentiviral transduction of the PaTu cell line to examine how the knockout of GATA6 modifies the protein expression. With Western Blot the protein expression was analyzed with anti-GATA6, anti-p63, anti-KRT14, anti-Vinculin, anti-E-cadherin, and anti-GAPDH-antibodies. The GATA6 expression levels were visibly lower, which confirmed a knockdown on the protein level. The levels of E-cadherin were slightly decreased, while KRT14 levels were slightly increased. The protein levels of p63 were higher upon GATA6 knockdown (Figure 27**Figure 23**A). These changes agree with the BXPC3 data (Figure 16), which shows the opposite for GATA6 overexpression. All changes, besides the protein levels of p63, were statistically significant as represented in Figure 27B.

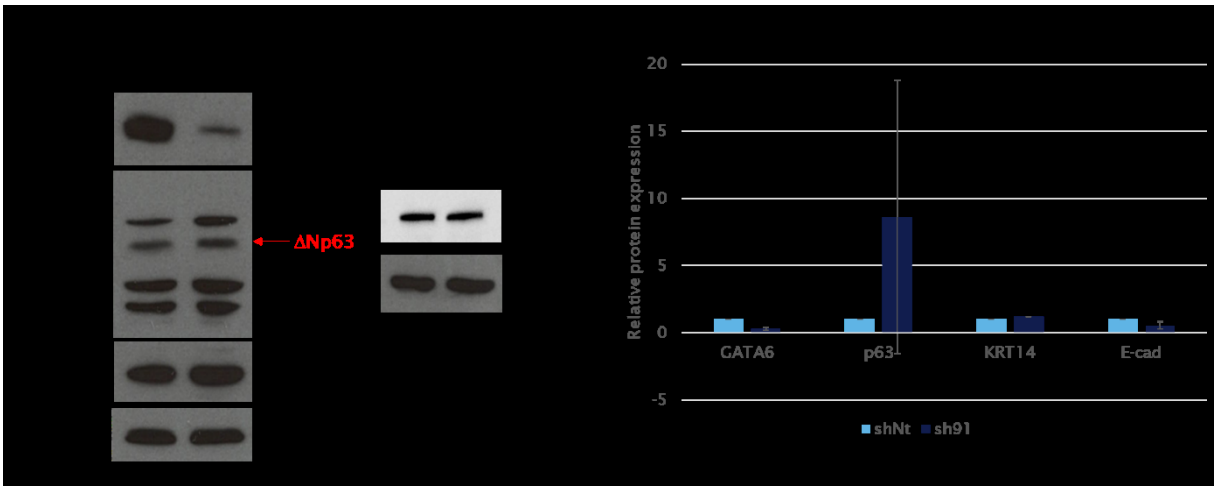

Figure 27: GATA6 knockdown leads to an increase in DNp63 and KRT14, while E-cadherin is downregulated. *[A] Stable non-target control (=shNt) and GATA6 knockdown (=sh91) PaTu cells were analyzed for differences in the protein levels of GATA6, p63, KRT14, and E-cadherin using Western Blot. Vinculin and GAPDH loading controls are indicated. [B] GATA6, p63, KRT14, and E-cadherin bands were quantified using ImageJ 1.52p software, normalized according to the loading controls, the relative to non-target control protein expression ratio was calculated and visualized using a chart diagram. Error bars represent the standard deviation of two independent experiments. Statistical analysis was performed using a two-tailed Student's t-test. *, p<0.05.*

8.3.2 Characterization of GATA6 knockdown effects on gene expression in PaTu cells

To assess how the GATA6 knockdown affects the gene expression in PaTu cells qPCR has been performed. Only GATA6 and ΔNp63 levels were examined due to time constraints since the establishment of the knockdown cell lines failed a few times and therefore the number of used primers for the characterization was subsequently decreased to a minimum. GATA6 downregulation was detectable and statistically significant on the gene expression level, confirming the knockdown (Figure 28). The basal-like gene ΔNp63 (orange), also showed a decrease (Figure 28), while an increase was observed on the protein level (Figure 27). Both modifications in the gene expression levels, however, are not of statistical significance.

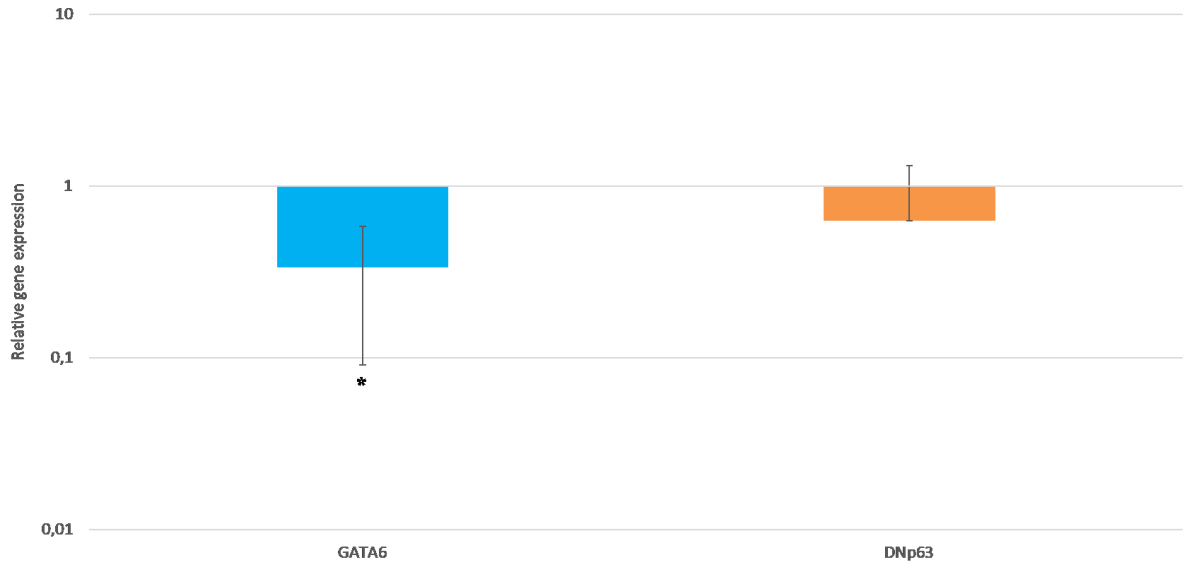

Figure 28: The mild increase in ΔNp63 on the protein level was not confirmed at the RNA level. *Differences in the gene expression levels of stable non-target control and GATA6 knockdown PaTu cells were detected using quantitative reverse transcriptase PCR. Gene expression levels were obtained as Ct values, normalized according to HPRT control, the relative to non-target control gene expression ratio was calculated and visualized using a chart diagram. Error bars represent the standard deviation of five independent experiments. Statistical analysis was performed using a two-tailed Student's t-test. *, p<0.05.*

8.3.3 Characterization of GATA6 knockdown effects on the chromatin in PaTu cells

8.3.3.1 Chromatin immunoprecipitation of the histone mark H3K27ac

PaTu cells were processed for ChIP-qPCR to investigate the changes in the chromatin landscape upon knockdown. The chromatin occupation levels of the histone mark H3K27ac were examined for ΔNp63, KRT14, GATA6, and negative control. A decrease of the histone mark H3K27ac was detected on the transcription start site of GATA6 in the knockdown cells. Consequently, the decrease of the basal-like genes (orange) suggests the concept that GATA6 knockdown decreases the levels of H3K27ac histone marks on the chromatin. The locus of ΔNp63 does not seem to be very active or to show any major epigenetic rearrangements in the PaTu cell line, compared to BXPC3 (Figure 21) and L3.6 (Figure 25). The knockdown of GATA6 also caused a decrease in H3K27ac on the negative control (red), underlining that the alterations of the acetylation of histone 3 on lysine 27 are not gene-specific (Figure 29).

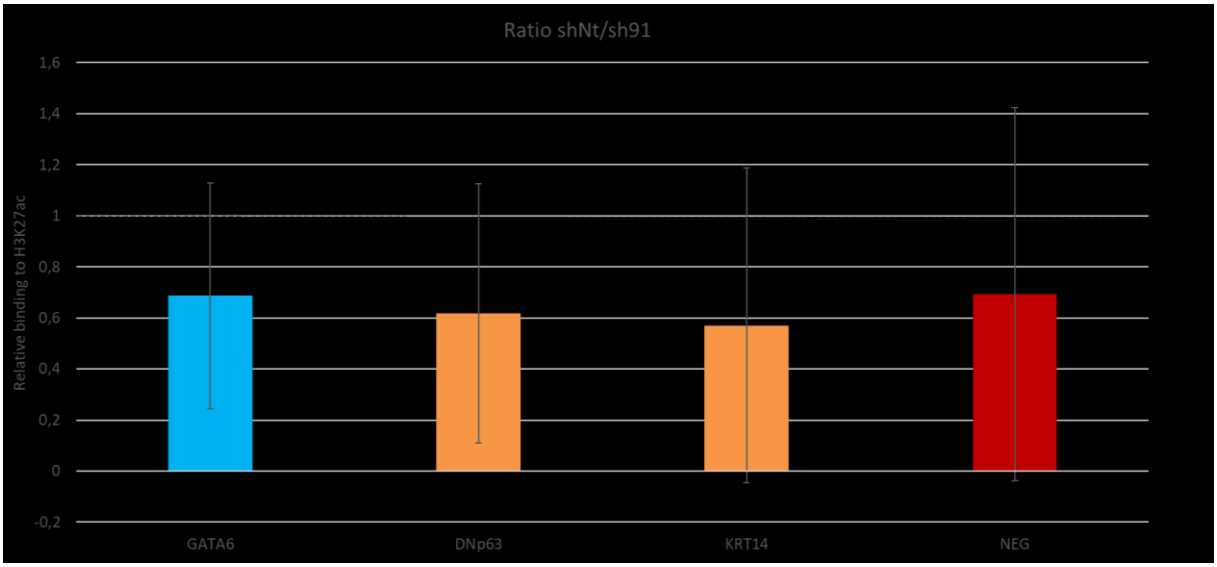

Figure 29: GATA6 knockdown reduces the openness of the GATA6 locus. *Stable non-target control and GATA6 knockdown PaTu cells were untreated and subsequently used for chromatin immunoprecipitation. Differences in the chromatin pulldown of H3K27ac in the indicated genes were detected using quantitative PCR. H3K27ac chromatin occupation levels were obtained*

*as Ct values, normalized according to the relative of non-target control chromatin occupation levels and visualized using a chart diagram. The error bars represent the standard deviation of three independent experiments. Statistical analysis was performed using a two-tailed Student's t-test. *, p<0.05.*

8.3.3.2 Chromatin immunoprecipitation of the transcription factor GATA6

The alterations on GATA6 chromatin occupancy levels were observed for PaTu knockdown cells with ChIP-qPCR. The same gene set as in 8.3.3.1 was examined for the GATA6-ChIP, namely: ΔNp63, KRT14, GATA6, and negative control. GATA6 knockdown led to a decrease of GATA6 occupying its own promoter (light blue). In general, as previously seen in Figure 29, the chromatin is generally less open upon GATA6 knockdown and also the binding of GATA6 to the chromatin is decreased. The promoter of the basal-like gene ΔNp63 shows almost no distinction in GATA6 binding when compared to the non-target control, which led to the conclusion that GATA6 does not bind to the promoter of ΔNp63. Based on this, the knockdown appears to not be efficient enough to switch the PaTu cells to the basal-like phenotype that has been observed in patient samples. The only conclusion by this data is that the promoter of ΔNp63 is not very active in the PaTu cell line. The KRT14 promoter showed a decrease in GATA6 similar to GATA6 itself and once more, the decrease was also detectable in the negative control (red). Mainly, it is possible to conclude that the knockdown of GATA6 reduces the binding of GATA6 (Figure 30).

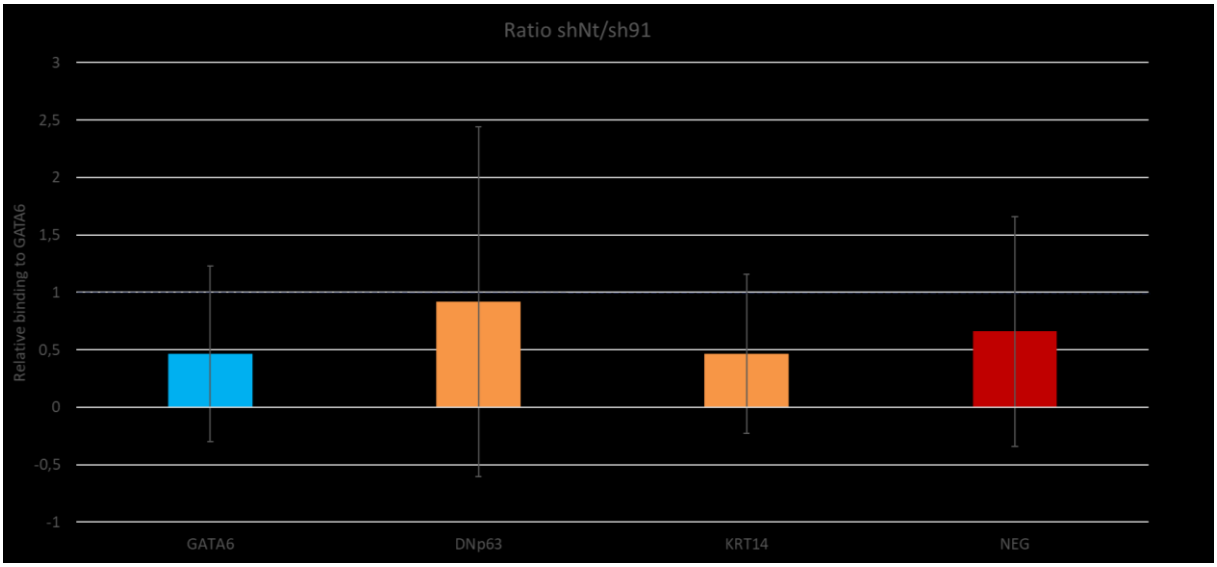

Figure 30: GATA6 knockdown reduces the binding of GATA6. *Stable non-target control and GATA6 knockdown PaTu cells were untreated and subsequently used for chromatin immunoprecipitation. Differences in the chromatin pulldown of GATA6 in the indicated genes were detected using quantitative PCR. GATA6 chromatin occupation levels were obtained as Ct values, normalized according to the relative of non-target control chromatin occupation levels and visualized using a chart diagram. The error bars represent the standard deviation of three independent experiments. Statistical analysis was performed using a two-tailed Student's t-test. *, p<0.05.*

9 Discussion

In this study, we show that two GATA6-overexpressing and one GATA6 knockdown PDAC cell lines were successfully generated and characterized in terms of the GATA6 overexpression and GATA6 knockdown effects on protein expression, gene expression and the chromatin landscape under normal conditions.

Western Blot experiments of BxPC-3 have shown results that were in concordance with the hypothesis, that when GATA6 expression increases, ΔNp63 and KRT14 are downregulated. Additionally, E-cadherin was upregulated, and all changes were statistically significant in four independent experiments. The data for the L3.6pl experiments showed to some extent a contrasting effect since ΔNp63 protein levels were increased in GATA6-overexpressing cells. However, none of the protein level changes of p63, KRT14, and E-cadherin were statistically significant in the L3.6pl overexpression models. Due to time constraints, the generation of a new L3.6pl overexpression cell line was not performed but would probably confirm these results and the model could be explored further or if yielding different results could be compared to the other two cell lines. What is also important to keep in mind is that the used cell lines are established and in 2D cell culture and therefore, might not behave like real PDAC; additional to harboring various mutational backgrounds leading to the confirmation of a hypothesis in one cell line but not in the other. For the PaTu8988S knockdown experiments, only two Western Blot experiments were quantifiable, since some bands, for example, the p63/ΔNp63, did not develop in every blot and cells tended to lose the knockdown. Largely, the opposite of the BxPC-3 data could be observed, though, not to the same extent. ΔNp63 and KRT14 were mildly increased upon knockdown of GATA6 in PaTu8988S cells, while E-cadherin levels decreased. Based on the very high difference of ΔNp63 basal levels between the two experiments, no statistical significance was detectable.

For the RT-qPCR experiments, different gene sets were analyzed for each cell line. The most extensive analysis was performed for the BxPC-3 cell line with 20 different primers amplifying classical, basal-like, and mesenchymal genes, as well as HPRT as a housekeeping gene control and GATA6 itself. In the BxPC-3 data, it seemed that there might be no link between the basal-like subtype and the EMT, since N-cadherin, a mesenchymal marker, was increased upon GATA6 overexpression, while the expression of all basal-like genes decreased. In addition, other EMT markers like SNAI1, SNAI2, VIM, and TWIST1 were analyzed but only showed moderate upregulation. Nonetheless, our data might suggest that the basal and the mesenchymal phenotypes are not necessarily linked to each other. This was not explored further or confirmed by us but could be an interesting follow-up. For the L3.6pl model, 17 primers were used, since mesenchymal genes like SNAI1, SNAI2, VIM, and TWIST1, have been previously checked in the same study in which the functional assays took place[13]. For the PaTu8988S knockdown model, the number of primers was ultimately decreased to GATA6, ΔNp63, and HPRT, to assess only if the knockdown was successful or not, centered on the many rounds of performed RT-qPCR experiments in which the data showed no efficient knockdown.

The functional assays were only performed in the empty vector and GATA6 overexpressing BxPC-3 cell lines since the laboratory already published data on the L3.6pl overexpression and on the PaTu8988S knockdown model. Overexpression of GATA6 in L3.6pl led to a decrease of invasiveness *in vitro* and *in vivo*, while knockdown of GATA6 in PaTu8988S led to an increase of invasiveness *in vitro* and *in vivo*[13]. In contrast, GATA6 overexpression in the BxPC-3 cell line did not appear to change *in vitro* proliferation, migration or invasion in a statistically significant manner. In general, it has been observed that the motility of BxPC-3 cells is low when compared to other cell lines *in vitro*. Similar results were measured *in vivo* when tumors took more than a month to establish upon subcutaneous injection[84]. Hence, it might be hard to see changes towards a lower proliferative, migratory or invasive potential, when the processes are already slow, to begin with.

In summary, with the ChIP experiments in which the histone mark H3K27ac was pulled down, we were able to observe more open chromatin upon GATA6 overexpression in BxPC-3 and L3.6pl cells, while

GATA6 knockdown in PaTu8988S lead to less open chromatin. For the BxPC-3 data, the data is statistically significant, even though standard deviations are high. For the other two cell lines, the standard deviations are so high that no statistically significant difference could be observed. Hence, the H3K27ac ChIP experiments should be repeated with newly transduced L3.6pl GATA6 overexpressing cells, as well as with newly transduced PaTu8988S GATA6 knockdown cells upon re-characterization. The second set of ChIP experiments focused on GATA6 itself. In this set of experiments, GATA6 appears to have direct and indirect targets across the genes that we analyzed. In the L3.6pl overexpression model, the changes are milder. Only ΔNp63 appeared to be affected directly, while TAp63 and KRT14 displayed binding values identical to the relative binding of the FG12 control. In the PaTu8988S knockdown model, a tendency of reduced GATA6 binding after knockdown of GATA6 is visible, at the same time GATA6 binding to ΔNp63 appears to be unchanged. The only conclusion, which we can take based on the ChIP data from the PaTu8988S model is that the locus of ΔNp63 is not very active and seems to be closed. GATA6 is not binding to the non-target control region. Consequently, we think that the knockdown was not efficient to switch the cells into the basal-like phenotype which is often observed in the patients with pancreatic cancer.

The main problem with the ChIP protocol is the many steps it consists of. A three-day protocol with multiple steps that cannot be well controlled or checked for quality is sensitive to small changes and can, therefore, lead to big variances in the resulting data. Therefore, it is not always possible to directly compare experiments with each other. Since the data presented in this study show at least two out of three ChIP experiments with very high variability between runs, additional care must be taken in the future to increase reproducibility. One bias that can easily be introduced into the data is by the cross-linking time. One study shows[85] that after long fixation with formaldehyde even GFP, which does not interact with DNA, can be retrieved by ChIP, and also that the cross-linking time should be drastically decreased for highly abundant proteins to minimize the risk of false-positive retrieval of protein-DNA interactions[85]. Also, the retrieval of high binding values for negative controls or isotype control pulldown can be introduced by this effect[86]. However, the study states that non-specific cross-linking is not an issue for human cell lines when the fixation time is held under 10 minutes[85]. In our study, we crosslinked for 10 minutes and also other H3K27ac-ChIP protocols[87–89] have been checked, which are using a time window of between 10 and 15 minutes for fixation. Therefore, this bias is most probably ruled out from our presented data.

One newer method that could be used instead of ChIP and reduces multiple of the mentioned caveats, is CUT&RUN (Cleavage Under Targets and Release Using Nuclease)[90,91]. The principle is based on the antibody-binding of the transcription factor and subsequent nuclease digestion. No fixation is necessary and the supernatant upon nuclease cutting can be used for the preparation of the sequencing library, making it possible to shorten the protocol to only one day[90,91]. Also Single Molecule Footprinting (SMF)[92] could be used for our purposes. With this method, it is possible to take a closer look at the single molecules and detect the percentage of bound protein to the DNA, since heterogeneity cannot be visualized in ChIP data, which is based on the bulk analysis of millions of cells[92].

The three PDAC cell lines used in this project harbor different mutations while also expressing different levels of endogenous GATA6. PaTu8988S cells have the highest internal GATA6 expression, therefore, we used this cell line, which has been categorized into the classical subtype for the knockdown experiments. The other two cell lines BxPC-3 and L3.6pl show low levels of GATA6 and were categorized into the basal-like subtype, based on this we used these cell lines for our overexpression model. The most frequent mutation in PDAC, found in more than 95% of the patients, is KRAS[5]. Strikingly, the cell line BxPC-3 harbors no KRAS mutations, which is atypical for pancreatic cancer. It has been derived from the pancreas of a 61-year-old woman, which suffered from PDAC, died six months after the cell line has been cultured, although no metastases were found. Additionally, the cell line has a homozygous deletion of SMAD4, wildtype CDKN2A and a mutation on the amino acid 220 in TP53. It is also one of the most commonly used PDAC cell lines and we were able to achieve the most

conclusive results with it, however, based on the wildtype KRAS the question remains if the results are illustrative for the majority of pancreatic tumors[84]. The cell line L3.6pl is a derivative of the cell line COLO 357, which has been isolated from a metastatic female PDAC patient at the age of 77 years. It was established by several reinjection cycles into the pancreas of nude mice after liver metastasis was found[93]. In contrast to BxPC-3 and normal for a PDAC cell line, it harbors a G12D KRAS mutation[94]. The third cell line, PaTu8988S, has been isolated from a liver metastasis of a 64-year-old female PDAC patient, harbors a G12V KRAS mutation as well as an R282W TP53 mutation and shows an epithelial-like phenotype with low migratory potential[95,96].

Due to the contrasts presented between the data of the BXPC3 and the L3.6 cells, it could be suggested that the relationship between GATA6 and ΔNp63 is context-dependent. When taking the different genetic backgrounds of the two cell lines into consideration, the context could be based on either the mutational signature or the metastasis status or both. Nevertheless, this is not the first time that context-dependency has been observed for mammalian transcription factors, Eeckhoute et al.[97] presented that the genome organization and interconnection of gene regulation pathways already lead to cell-type and context-dependencies, but most probably there are modifications in epigenetic marks that are delivering the context for the transcription factors[97]. A closer look at the differences between the two overexpression model cell lines would be necessary to analyze the context.

The use of the overexpression system based on the FG12 vector showed efficient protein and gene expression levels of GATA6 in both used cell lines. The cell sorting for GFP-positive cells was a good tool to distinguish the right population that implemented the transduced plasmid. However, what we were able to observe, was that after multiple cell passaging steps the cells tended to lose the plasmid and a lower percentage of GFP-positive cells were detected when checked on the fluorescence microscope. Consequently, cells that were frozen after the cell sorting were thawed, when levels of GATA6 overexpression went down. It would have also been possible to re-sort or repeat the transduction. Also, the shRNA knockdown of GATA6 was efficient on the protein as well as on the gene expression level in the end and in the data shown in the Results section. Unfortunately, the generation of the knockdown was problematic, since the Puromycin selection over the weekend, which we used for the first transduction cycle did not seem to yield us a stable cell population with the GATA6 knockdown. The knockdown was lost after a few passages. Afterward, for the next knockdown experiment, the selection with Puromycin was prolonged to a week and ultimately for the last knockdown cell line, which was established, until 24 hours prior to experiments. Remarkably, this cell line also showed the loss of the knockdown and expressed GATA6 to almost the same extent as the non-target control after about two months in culture. All cell lines were previously checked for overexpression or knockdown and only if confirmed, further processed for ChIP experiments. Based on the acquired data it appears that the knockdown was not efficient enough to shift the cells into the basal-like phenotype.

The findings presented herein indicate that GATA6 plays a pivotal role in the regulation of the molecular phenotypes. The specific pathway, however, could not be confirmed. The BxPC-3 experiments confirm the downregulation of ΔNp63 through GATA6 overexpression. As a consequence, also the basal-like program seems to be downregulated. However, based on the ChIP data the modulation does not seem to be initiated by the changes in the chromatin landscape. Due to a different signature of GATA6-overexpressing L3.6pl cells across protein and gene expression, as well as the chromatin occupancy, the connection between GATA6 and ΔNp63 seems to be context-dependent. Even though the data is not as clear, the PaTu8988S knockdown model shows an upregulation of ΔNp63 upon GATA6 knockdown, which is the contrary to what has been observed in the BxPC-3 overexpression models. These two models can be compared to each other and confirmed, while the L3.6pl GATA6-overexpressing cells, or the L3.6pl cells in general, should be analyzed more closely to assess where the specificity of the ΔNp63 response is coming from.

Additionally, new transductions should be performed for the L3.6pl overexpression model, as well as for the PaTu8988S knockdown model. Then the characterization would need to be conducted again before following up with ChIP experiments. However, the use of a second knockdown model would be of advantage, by using a different cell line, based on our knowledge, PaTu8988S was the only cell line categorized into the classical subtype. Nonetheless, also trying a knockout approach with CRISPR/Cas could help to achieve a stable phenotype, since the shRNA approach did not appear to be permanent in our case. But as previously mentioned, it is normal that cell lines show changes after multiple passaging. It would be also interesting to change the method with which we assessed the changes in the chromatin landscape. The most promising methods for the analysis of protein-DNA interactions would be CUT&RUN (Cleavage Under Targets and Release Using Nuclease)[90,91] or Single Molecule Footprinting (SMF)[92], which would both help to decrease the bulk effect in the processed samples. One follow-up towards another direction would be the further exploration of the link between the basal-like subtype and EMT, which, based on our preliminary data in the BxPC-3 GATA6 overexpression model; did not appear to be interconnected to each other. Another path could focus on the differences between the two overexpression model cell lines, BxPC-3 and L3.6pl, to achieve a clearer picture of the necessary context for the GATA6 and ΔNp63 link.

With this study, the direct correlation of GATA6 and ΔNp63 should have been investigated since these two have been linked to either the classical or the basal-like subtype, respectively, but to our knowledge have not been linked to each other yet. With the BxPC-3 overexpression and the PaTu knockdown model of GATA6, we were able to confirm our hypothesis that GATA6 and ΔNp63 have an indirectly proportional relationship. The L3.6 cell line could not deliver the same confirmation of our hypothesis, nonetheless, additional insight was achieved since it became evident that the link appears to be dependent on a specific context in the cells. This could be the starting point for further research given that this context is most probably connected to PDAC's heterogeneity and could help to elucidate the different therapy responses in patients upon treatment. In addition, also the separation of the basal-like subtype and EMT, which was noticed in the BxPC-3 overexpression model, could be used for more effective or even personalized therapy in the future after further thorough investigation.

10 Conclusion

The project had the aim to study GATA6's role in the regulation of epigenetic changes, especially linked to the ΔNp63-driven basal phenotype in PDAC. The relationship between GATA6 and ΔNp63 could not be fully explored by our experiments and would need further analysis.

10.1 BxPC-3 GATA6 overexpression model

This model was able to give us the clearest data. GATA6 overexpression does not influence the growth rate, migration or invasion in BxPC-3 cells overexpressing GATA6 in comparison to empty vector control cells. Also, when GATA6 expression is increased, the downregulation of ΔNp63 and Krt14 can be observed, while E-cadherin levels are increased. These changes were confirmed on the protein as well as on the gene expression level. The chromatin seems to be generally more open when GATA6 is overexpressed, this, however, is not gene-specific. The GATA6 binding seems to have direct and indirect targets, but generally also shows increased binding. The tendency to have more open chromatin could lead to more GATA6 binding or it could be vice versa, though, this was not explored.

GATA6↑ → ΔNp63↓ → KRT14↓

10.2 L3.6pl GATA6 overexpression model

This model behaved differently to the BxPC-3 cells. Some interesting contrasting effects were observed, however, due to time constraints could not be explored further. GATA6 overexpression leads to an increase in ΔNp63, a minimal decrease in Krt14 and an increase in E-cadherin. Krt14 and E-cadherin are in concordance with the BxPC-3 overexpression model, nonetheless, the upregulation of p63 hints that the GATA6 function might be dependent on the context. None of these show a significant change in protein or gene expression. The only significant upregulations on the gene expression level are the upregulation of FOXA2 and FAT2. The chromatin seems to be, also in this model, generally more open upon GATA6 overexpression and lacks specificity. Remarkably, when assessing GATA6 binding to the promoters an increase in binding to ΔNp63 is observable, probably leading to the activation of ΔNp63, the other changes seem to be indirectly.

GATA6↑ → ΔNp63↑? → KRT14↓

10.3 PaTu8988S GATA6 knockdown model

GATA6 knockdown led to a mild increase in ΔNp63 and Krt14 on the protein level. The increase of Krt14 is significant, as well as the decrease of E-cadherin. This data supports the BxPC-3 overexpression model since it shows the opposite. Unfortunately, due to time constraints, the panel of primers for RT-qPCR was reduced, therefore, the just mentioned changes have not been confirmed on the RNA level. All in all, GATA6 knockdown tends to reduce the openness of the chromatin and a tendency of reduced GATA6 binding after knockdown of GATA6 is visible, at the same time GATA6 binding to ΔNp63 appears to be unchanged. The locus of ΔNp63 is not very active and seems to be closed. Consequently, we think that the knockdown was not efficient to switch the cells into the basal-like phenotype which is often observed in the patients with pancreatic cancer.

GATA6↓ → ΔNp63↑ → KRT14↑

11 References

1. Ferlay J, Soerjomataram I, Ervik M, Dikshit R, Eser S, Mathers C, et al. *GLOBOCAN 2012 v1.0, Cancer Incidence and Mortality Worldwide: IARC CancerBase No. 11*. (2013).
2. Bray, F. *et al.* Global cancer statistics 2018: GLOBOCAN estimates of incidence and mortality worldwide for 36 cancers in 185 countries. *CA. Cancer J. Clin.* **68**, 394–424 (2018).
3. Siegel, R. L., Miller, K. D. & Jemal, A. Cancer statistics, 2018. *CA. Cancer J. Clin.* **68**, 7–30 (2018).
4. 5 Year Cancer Survival Rates - 1975 Vs 2003. Available at: http://healthhubs.net/images/cancer-survival-trends.gif. (Accessed: 9th August 2019)
5. Morris, J. P., Wang, S. C. & Hebrok, M. KRAS, Hedgehog, Wnt and the twisted developmental biology of pancreatic ductal adenocarcinoma. *Nat. Rev. Cancer* **10**, 683–695 (2010).
6. Gopinathan, A., Morton, J. P., Jodrell, D. I. & Sansom, O. J. GEMMs as preclinical models for testing pancreatic cancer therapies. *Dis. Model. Mech.* **8**, 1185–200 (2015).
7. O'Hagan, R. C. & Heyer, J. KRAS Mouse Models: Modeling Cancer Harboring KRAS Mutations. *Genes Cancer* **2**, 335–43 (2011).
8. Hingorani, S. R. *et al.* Trp53R172H and KrasG12D cooperate to promote chromosomal instability and widely metastatic pancreatic ductal adenocarcinoma in mice. *Cancer Cell* **7**, 469–83 (2005).
9. Lee, J. W., Komar, C. A., Bengsch, F., Graham, K. & Beatty, G. L. Genetically Engineered Mouse Models of Pancreatic Cancer: The KPC Model (LSL-Kras(G12D/+) ;LSL-Trp53(R172H/+) ;Pdx-1-Cre), Its Variants, and Their Application in Immuno-oncology Drug Discovery. *Curr. Protoc. Pharmacol.* **73**, 14.39.1-14.39.20 (2016).
10. Kamisawa, T., Wood, L. D., Itoi, T. & Takaori, K. Pancreatic cancer. *Lancet* **388**, 73–85 (2016).
11. Moffitt, R. A. *et al.* Virtual microdissection identifies distinct tumor- and stroma-specific subtypes of pancreatic ductal adenocarcinoma. *Nat. Genet.* **47**, 1168–1178 (2015).
12. Martinelli, P. *et al.* The acinar regulator Gata6 suppresses KrasG12V-driven pancreatic tumorigenesis in mice. *Gut* **65**, 476–86 (2015).
13. Martinelli, P. *et al.* GATA6 regulates EMT and tumour dissemination, and is a marker of response to adjuvant chemotherapy in pancreatic cancer. *Gut* **66**, 1665–1676 (2016).
14. Bhaw-Luximon, A. & Jhurry, D. New avenues for improving pancreatic ductal adenocarcinoma (PDAC) treatment: Selective stroma depletion combined with nano drug delivery. *Cancer Lett.* **369**, 266–273 (2015).
15. Kota, J., Hancock, J., Kwon, J. & Korc, M. Pancreatic cancer: Stroma and its current and emerging targeted therapies. *Cancer Lett.* **391**, 38–49 (2017).
16. Rhim, A. D. *et al.* Stromal Elements Act to Restrain, Rather Than Support, Pancreatic Ductal Adenocarcinoma. *Cancer Cell* **25**, 735–747 (2014).
17. Özdemir, B. C. *et al.* Depletion of carcinoma-associated fibroblasts and fibrosis induces immunosuppression and accelerates pancreas cancer with reduced survival. *Cancer Cell* **25**, 719–34 (2014).
18. Adamska, A., Domenichini, A. & Falasca, M. Pancreatic Ductal Adenocarcinoma: Current and Evolving Therapies. *Int. J. Mol. Sci.* **18**, 1338 (2017).
19. Garrido-Laguna, I. & Hidalgo, M. Pancreatic cancer: from state-of-the-art treatments to promising novel therapies. *Nat. Rev. Clin. Oncol.* **12**, 319–334 (2015).
20. Longley, D. B., Harkin, D. P. & Johnston, P. G. 5-Fluorouracil: mechanisms of action and clinical strategies. *Nat. Rev. Cancer* **3**, 330–338 (2003).
21. Structure of 5-FU. Available at: https://upload.wikimedia.org/wikipedia/commons/9/9b/Fluorouracil2DACS.svg. (Accessed: 4th September 2019)
22. Burris, H. A. *et al.* Improvements in survival and clinical benefit with gemcitabine as first-line therapy for patients with advanced pancreas cancer: a randomized trial. *J. Clin. Oncol.* **15**, 2403–2413 (1997).
23. Plunkett, W. *et al.* Gemcitabine: metabolism, mechanisms of action, and self-potentiation. *Semin. Oncol.* **22**, 3–10 (1995).

24. Structure of gemcitabine. Available at: https://upload.wikimedia.org/wikipedia/commons/f/ff/Gemcitabine.svg. (Accessed: 4th September 2019)
25. Conroy, T. *et al.* FOLFIRINOX versus Gemcitabine for Metastatic Pancreatic Cancer. *N. Engl. J. Med.* **364**, 1817–1825 (2011).
26. Von Hoff, D. D. *et al.* Increased Survival in Pancreatic Cancer with nab-Paclitaxel plus Gemcitabine. *N. Engl. J. Med.* **369**, 1691–1703 (2013).
27. FOLFIRINOX Therapy Scheme. Available at: https://www.pancreaticcancer.org.uk/media/1119548/folfirinox-chemotherapy-cycle.jpg. (Accessed: 4th September 2019)
28. Nab-paclitaxel Therapy scheme. Available at: https://www.pancreaticcancer.org.uk/media/1119552/oxaliplatin-with-5-fu-and-folinic-acid-folfox-chemotherapy-cycle.jpg. (Accessed: 4th September 2019)
29. Eser, S., Schnieke, A., Schneider, G. & Saur, D. Oncogenic KRAS signalling in pancreatic cancer. *Br. J. Cancer* **111**, 817–822 (2014).
30. Collins, M. A. *et al.* Oncogenic Kras is required for both the initiation and maintenance of pancreatic cancer in mice. *J. Clin. Invest.* **122**, 639–653 (2012).
31. Waters, A. M. & Der, C. J. KRAS: The Critical Driver and Therapeutic Target for Pancreatic Cancer. *Cold Spring Harb. Perspect. Med.* **8**, a031435 (2018).
32. Moore, M. J. *et al.* Erlotinib Plus Gemcitabine Compared With Gemcitabine Alone in Patients With Advanced Pancreatic Cancer: A Phase III Trial of the National Cancer Institute of Canada Clinical Trials Group. *J. Clin. Oncol.* **25**, 1960–1966 (2007).
33. Philip, P. A. *et al.* Phase III Study Comparing Gemcitabine Plus Cetuximab Versus Gemcitabine in Patients With Advanced Pancreatic Adenocarcinoma: Southwest Oncology Group–Directed Intergroup Trial S0205. *J. Clin. Oncol.* **28**, 3605–3610 (2010).
34. Kindler, H. L. *et al.* Axitinib plus gemcitabine versus placebo plus gemcitabine in patients with advanced pancreatic adenocarcinoma: a double-blind randomised phase 3 study. *Lancet. Oncol.* **12**, 256–62 (2011).
35. Ioka, T. *et al.* Efficacy and safety of axitinib in combination with gemcitabine in advanced pancreatic cancer: subgroup analyses by region, including Japan, from the global randomized Phase III trial. *Jpn. J. Clin. Oncol.* **45**, 439–448 (2015).
36. Kindler, H. L. *et al.* Phase II Trial of Bevacizumab Plus Gemcitabine in Patients With Advanced Pancreatic Cancer. *J. Clin. Oncol.* **23**, 8033–8040 (2005).
37. Zhang, Y. *et al.* Myeloid cells are required for PD-1/PD-L1 checkpoint activation and the establishment of an immunosuppressive environment in pancreatic cancer. *Gut* **66**, 124–136 (2017).
38. Brahmer, J. R. *et al.* Safety and Activity of Anti–PD-L1 Antibody in Patients with Advanced Cancer. *N. Engl. J. Med.* **366**, 2455–2465 (2012).
39. Beatty, G. L. *et al.* CD40 Agonists Alter Tumor Stroma and Show Efficacy Against Pancreatic Carcinoma in Mice and Humans. *Science (80-.).* **331**, 1612–1616 (2011).
40. Vonderheide, R. H. *et al.* CD40 immunotherapy for pancreatic cancer. *Cancer Immunol. Immunother.* **62**, 949–954 (2013).
41. Garrido-Laguna, I. & Hidalgo, M. Pancreatic cancer: from state-of-the-art treatments to promising novel therapies. *Nat. Rev. Clin. Oncol.* **12**, 319–334 (2015).
42. Madden, J. I. Infinity Reports Update from Phase 2 Study of Saridegib Plus Gemcitabine in Patients with Metastatic Pancreatic Cancer | Business Wire. Available at: https://www.businesswire.com/news/home/20120127005146/en/Infinity-Reports-Update-Phase-2-Study-Saridegib. (Accessed: 28th August 2019)
43. Von Hoff, D. *et al.* O-0003 * NAPOLI-1: RANDOMIZED PHASE 3 STUDY OF MM-398 (NAL-IRI), WITH OR WITHOUT 5-FLUOROURACIL AND LEUCOVORIN, VERSUS 5-FLUOROURACIL AND LEUCOVORIN, IN METASTATIC PANCREATIC CANCER PROGRESSED ON OR FOLLOWING GEMCITABINE-BASED THERAPY. *Ann. Oncol.* **25**, ii105–ii106 (2014).
44. Boone, B. A. *et al.* Safety and Biologic Response of Pre-operative Autophagy Inhibition in

Combination with Gemcitabine in Patients with Pancreatic Adenocarcinoma. *Ann. Surg. Oncol.* **22**, 4402–10 (2015).
45. Bahary, N. Randomized Phase II Trial of Pre-Operative Gemcitabine and Nab Paclitacel With or With Out Hydroxychloroquine. (2019). Available at: https://clinicaltrials.gov/ct2/show/study/NCT01978184. (Accessed: 28th August 2019)
46. Karasic, T. B. *et al.* Effect of Gemcitabine and nab-Paclitaxel With or Without Hydroxychloroquine on Patients With Advanced Pancreatic Cancer. *JAMA Oncol.* **5**, 993 (2019).
47. O'Dwyer, P. A Phase I/II/Pharmacodynamic Study of Hydroxychloroquine in Combination With Gemcitabine/Abraxane to Inhibit Autophagy in Pancreatic Cancer. (2019). Available at: https://clinicaltrials.gov/ct2/show/NCT01506973. (Accessed: 28th August 2019)
48. Neureiter, D., Jäger, T., Ocker, M. & Kiesslich, T. Epigenetics and pancreatic cancer: pathophysiology and novel treatment aspects. *World J. Gastroenterol.* **20**, 7830–48 (2014).
49. Hessmann, E., Johnsen, S. A., Siveke, J. T. & Ellenrieder, V. Epigenetic treatment of pancreatic cancer: is there a therapeutic perspective on the horizon? *Gut* **66**, 168–179 (2017).
50. Paradise, B. D., Barham, W. & Fernandez-Zapico, M. E. Targeting Epigenetic Aberrations in Pancreatic Cancer, a New Path to Improve Patient Outcomes? *Cancers (Basel).* **10**, (2018).
51. Natale, F., Vivo, M., Falco, G. & Angrisano, T. Deciphering DNA methylation signatures of pancreatic cancer and pancreatitis. *Clin. Epigenetics* **11**, 132 (2019).
52. Bailey, P. *et al.* Genomic analyses identify molecular subtypes of pancreatic cancer. *Nature* **531**, 47–52 (2016).
53. Andricovich, J. *et al.* Loss of KDM6A Activates Super-Enhancers to Induce Gender-Specific Squamous-like Pancreatic Cancer and Confers Sensitivity to BET Inhibitors. *Cancer Cell* **33**, 512-526.e8 (2018).
54. Somerville, T. D. D. *et al.* TP63-Mediated Enhancer Reprogramming Drives the Squamous Subtype of Pancreatic Ductal Adenocarcinoma. *Cell Rep.* **25**, 1741-1755.e7 (2018).
55. Hamdan, F., Johnsen, S., Hamdan, F. H. & Johnsen, S. A. Epigenetic Targeting of Aberrant Transcriptional Modulation in Pancreatic Cancer. *Epigenomes* **2**, 8 (2018).
56. GRØNBAEK, K., HOTHER, C. & JONES, P. A. Epigenetic changes in cancer. *APMIS* **115**, 1039–1059 (2007).
57. Fardi, M., Solali, S. & Farshdousti Hagh, M. Epigenetic mechanisms as a new approach in cancer treatment: An updated review. *Genes Dis.* **5**, 304–311 (2018).
58. Lansdowne, L. E. Epigenetics and Drug Discovery. (2018). Available at: https://www.technologynetworks.com/drug-discovery/articles/epigenetics-and-drug-discovery-306821. (Accessed: 10th September 2019)
59. Juiz, N. A., Iovanna, J. & Dusetti, N. Pancreatic Cancer Heterogeneity Can Be Explained Beyond the Genome. *Front. Oncol.* **9**, 246 (2019).
60. Collisson, E. A. *et al.* Subtypes of pancreatic ductal adenocarcinoma and their differing responses to therapy. *Nat. Med.* **17**, 500–503 (2011).
61. Puleo, F. *et al.* Stratification of Pancreatic Ductal Adenocarcinomas Based on Tumor and Microenvironment Features. *Gastroenterology* **155**, 1999-2013.e3 (2018).
62. Cancer Genome Atlas Research Network. Electronic address: andrew_aguirre@dfci.harvard.edu, B. J. *et al.* Integrated Genomic Characterization of Pancreatic Ductal Adenocarcinoma. *Cancer Cell* **32**, 185-203.e13 (2017).
63. Birnbaum, D. J., Finetti, P., Birnbaum, D., Mamessier, E. & Bertucci, F. Validation and comparison of the molecular classifications of pancreatic carcinomas. *Mol. Cancer* **16**, 168 (2017).
64. Connor, A. A. *et al.* Integration of Genomic and Transcriptional Features in Pancreatic Cancer Reveals Increased Cell Cycle Progression in Metastases. *Cancer Cell* **35**, 267-282.e7 (2019).
65. Decker, K., Goldman, D. C., L. Grasch, C. & Sussel, L. Gata6 is an important regulator of mouse pancreas development. *Dev. Biol.* **298**, 415–429 (2006).
66. Xuan, S. & Sussel, L. GATA4 and GATA6 regulate pancreatic endoderm identity through inhibition of hedgehog signaling. *Development* **143**, 780–6 (2016).

67. Tiyaboonchai, A. *et al.* GATA6 Plays an Important Role in the Induction of Human Definitive Endoderm, Development of the Pancreas, and Functionality of Pancreatic β Cells. *Stem cell reports* **8**, 589–604 (2017).
68. Seino, T. *et al.* Human Pancreatic Tumor Organoids Reveal Loss of Stem Cell Niche Factor Dependence during Disease Progression. *Cell Stem Cell* **22**, 454-467.e6 (2018).
69. Real, F. X., Vilá, M. R., Skoudy, A., Ramaekers, F. C. S. & Corominas, J. M. Intermediate filaments as differentiation markers of exocrine pancreas. II. Expression of cytokeratins of complex and stratified epithelia in normal pancreas and in pancreas cancer. *Int. J. Cancer* **54**, 720–727 (1993).
70. Adams, C. R. *et al.* Transcriptional control of subtype switching ensures adaptation and growth of pancreatic cancer. *Elife* **8**, (2019).
71. Tremblay, M., Sanchez-Ferras, O. & Bouchard, M. GATA transcription factors in development and disease. *Development* **145**, dev164384 (2018).
72. Merika, M. & Orkin, S. H. DNA-binding specificity of GATA family transcription factors. *Mol. Cell. Biol.* **13**, 3999–4010 (1993).
73. Iwafuchi-Doi, M. & Zaret, K. S. Pioneer transcription factors in cell reprogramming. *Genes Dev.* **28**, 2679–92 (2014).
74. Wamaitha, S. E. *et al.* Gata6 potently initiates reprograming of pluripotent and differentiated cells to extraembryonic endoderm stem cells. *Genes Dev.* **29**, 1239–55 (2015).
75. Morrisey, E. E. *et al.* GATA6 regulates HNF4 and is required for differentiation of visceral endoderm in the mouse embryo. *Genes Dev.* **12**, 3579–3590 (1998).
76. Lentjes, M. H. F. M. *et al.* The emerging role of GATA transcription factors in development and disease. *Expert Rev. Mol. Med.* **18**, e3 (2016).
77. Lomberk, G. *et al.* Distinct epigenetic landscapes underlie the pathobiology of pancreatic cancer subtypes. *Nat. Commun.* **9**, 1978 (2018).
78. Molin, M. D. *et al.* Very Long-term Survival Following Resection for Pancreatic Cancer Is Not Explained by Commonly Mutated Genes: Results of Whole-Exome Sequencing Analysis. *Clin. Cancer Res.* **21**, 1944–1950 (2015).
79. Reichert, M. *et al.* Regulation of Epithelial Plasticity Determines Metastatic Organotropism in Pancreatic Cancer. *Dev. Cell* **45**, 696-711.e8 (2018).
80. Keyes, W. M. *et al.* ΔNp63α is an oncogene that targets chromatin remodeler Lsh to drive skin stem cell proliferation and tumorigenesis. *Cell Stem Cell* **8**, 164–76 (2011).
81. Soares, E. & Zhou, H. Master regulatory role of p63 in epidermal development and disease. *Cell. Mol. Life Sci.* **75**, 1179–1190 (2018).
82. Tan, E. H. *et al.* Functions of TAp63 and p53 in restraining the development of metastatic cancer. *Oncogene* **33**, 3325–33 (2014).
83. UniProtKB/Swiss-Prot. UniProtKB - Q9H3D4 (P63_HUMAN). *2019* Available at: https://www.uniprot.org/uniprot/Q9H3D4. (Accessed: 13th September 2019)
84. Deer, E. L. *et al.* Phenotype and Genotype of Pancreatic Cancer Cell Lines. *Pancreas* **39**, 425–435 (2010).
85. Baranello, L., Kouzine, F., Sanford, S. & Levens, D. ChIP bias as a function of cross-linking time. *Chromosom. Res.* **24**, 175–181 (2016).
86. Marinov, G. K., Kundaje, A., Park, P. J. & Wold, B. J. Large-scale quality analysis of published ChIP-seq data. *G3 (Bethesda).* **4**, 209–23 (2014).
87. Peters, A. H. F. M. *et al.* Partitioning and plasticity of repressive histone methylation states in mammalian chromatin. *Mol. Cell* **12**, 1577–89 (2003).
88. Creyghton, M. P. *et al.* Histone H3K27ac separates active from poised enhancers and predicts developmental state. *Proc. Natl. Acad. Sci. U. S. A.* **107**, 21931–6 (2010).
89. Tamura, I. *et al.* Genome-wide analysis of histone modifications in human endometrial stromal cells. *Mol. Endocrinol.* **28**, 1656–69 (2014).
90. Skene, P. J. & Henikoff, S. An efficient targeted nuclease strategy for high-resolution mapping of DNA binding sites. *Elife* **6**, (2017).
91. Skene, P. J., Henikoff, J. G. & Henikoff, S. Targeted in situ genome-wide profiling with high

efficiency for low cell numbers. *Nat. Protoc.* **13**, 1006–1019 (2018).
92. Krebs, A. R. *et al.* Genome-wide Single-Molecule Footprinting Reveals High RNA Polymerase II Turnover at Paused Promoters. *Mol. Cell* **67**, 411-422.e4 (2017).
93. Bruns, C. J., Harbison, M. T., Kuniyasu, H., Eue, I. & Fidler, I. J. In Vivo Selection and Characterization of Metastatic Variants from Human Pancreatic Adenocarcinoma by Using Orthotopic Implantation in Nude Mice. *Neoplasia* **1**, 50–62 (1999).
94. SIB Swiss Institute of Bioinformatics. Cellosaurus L3.6pl (CVCL_0384). Available at: https://web.expasy.org/cellosaurus/CVCL_0384. (Accessed: 13th September 2019)
95. SIB Swiss Institute of Bioinformatics. Cellosaurus PaTu 8988s (CVCL_1846). Available at: https://web.expasy.org/cellosaurus/CVCL_1846. (Accessed: 13th September 2019)
96. Marques, I. J. *et al.* Metastatic behaviour of primary human tumours in a zebrafish xenotransplantation model. *BMC Cancer* **9**, 128 (2009).
97. Eeckhoute, J., Métivier, R. & Salbert, G. Defining specificity of transcription factor regulatory activities. *J. Cell Sci.* **122**, 4027–34 (2009).

12 Appendix

12.1 List of abbreviations

Abbreviation	Explanation
°C	Degrees Celsius
µL	Microliter
2D cell culture	Two-dimensional Cell Culture
5-FU	5-Fluorouracil
ADEX	Aberrantly Differentiated Endocrine Exocrine
Akt	Protein kinase B (PKB)
ATM	Ataxia Telangiectasia Mutated Gene
BET	Bromodomain and Extra-Terminal Motif
BrdU	Bromodeoxyuridine
BSA	Bovine Serum Albumin
BXPC3	BxPC-3
BxPC-3	Biopsy Xenograft of Pancreatic Carcinoma Line-3
CAR T cell therapy	Chimeric Antigen Receptor T cell therapy
CD40	Cluster of Differentiation 40
CDH1	E-cadherin
CDH2	N-cadherin
CDKN2A	Cyclin-Dependent Kinase Inhibitor 2A
cDNA	Complementary Deoxyribonucleic acid
ChIP	Chromatin Immunoprecipitation
ChIP-seq	Chromatin Immunoprecipitation sequencing
Cre	Cre recombinase
Ct values	Cycle Threshold Values
CUT&RUN	Cleavage Under Targets and Release Using Nuclease
DAPI	4',6-Diamidino-2-Phenylindole
DMEM	Dulbecco's Modified Eagle Medium
DMSO	Dimethyl Sulfoxide
DNA	Deoxyribonucleic acid
Dr.	Doctor
E9.5-10	Mouse Embryonic Day 9.5-10
E-cad	E-cadherin
EDTA	Ethylenediaminetetraacetic Acid
EGFR	Epidermal Growth Factor Receptor
EGTA	Ethylene Glycol-bis(β-aminoethyl ether)-N,N,N',N'-tetraacetic Acid
EMT	Epithelial-mesenchymal Transition
FAT2	FAT Atypical Cadherin 2
FBS	Fetal Bovine Serum
FG12	Empty Overexpression Vector
FG12-GATA6	GATA6 Overexpression Vector
FOLFIRINOX	Irinotecan, Oxaliplatin, 5-Fluorouracil, and Leucovorin
FOXA1	Forkhead Box Protein A1
FOXA2	Forkhead Box Protein A2
g	Relative Centrifugal Force
G12D	Glycine to Aspartic Acid Substitution at Position 12

G12V	Glycine to Valine Substitution at Position 12
GAPDH	Glyceraldehyde 3-phosphate Dehydrogenase
GATA6	GATA-binding factor 6
GEMM	Genetically engineered mouse models
GFP	Green Fluorescent Protein
GLI1	Human Glioma-Associated Oncogene Homolog 1
GLI2	Human Glioma-Associated Oncogene Homolog 2
GSEA	Gene Set Enrichment Analysis
H3K27ac	Histone 3 Lysine 27 Acetylation
H3K27me3	Histone 3 Lysine 27 Trimethylation
HCl	Hydrogen Chloride
HDAC	Histone Deacetylase
HEK293FT	Tumor Protein 293FT
HH	Hedgehog
Hh	Hedgehog
HNF4A	Hepatocyte Nuclear Factor 4 Alpha
HPRT	Hypoxanthine Phosphoribosyltransferase
INK4A	**IN**hibitors of CD**K4**
JAK3	Janus Kinase 3
KDM6A	Lysine Demethylase 6A
KIT	Mast/stem cell growth factor receptor (SCFR)
KLF5	Krüppel Like Factor 5
KO	Knock-Out
KOH	Potassium Hydroxide
KPC mouse model	mutated KRASG12D allele, heterozygous p53 mutation (R172H) and expression of Pdx-1-Cre
KRAS	Kirsten Rat Sarcoma Viral Oncogene Homolog
KRT14	Keratin 14
KRT14	Keratin 14
Krt19	Keratin 19
KRT5	Keratin 5
L3.6	L3.6pl
L3.6pl	L3.6 pancreas-liver
LiCl	Lithium Chloride
M.Sc.	Master of Science
MAPK	Mitogen-activated Protein Kinase
MET	Hepatocyte Growth Factor Receptor (HGFR)
mL	Milliliter
mM	Millimole
MM-398	Nanoliposomal Irinotecan
mTOR	Mammalian Target of Rapamycin
MYC	MYC Proto-oncogene
NaAc	Sodium Acetate
NaCl	Sodium Chloride
NAHCO3	Sodium Hydrogen Carbonate
Nat Gen	Nature Genetics
Nat Med	Nature Medicine

NECTIN1	Nectin Cell Adhesion Molecule 1
NEG	Negative Control
OPN	Osteopontin
p53	Tumor Protein 53
p63	Tumor Protein 63
PanINs	Pancreatic Intraepithelial Neoplasias
PaTu	PaTu8988S
PaTu8988S	Pancreatic Tumor 8988S
PBS	Phosphate-buffered Saline
PCR	Polymerase Chain Reaction
PD-1	Programmed death receptor 1
PDAC	Pancreatic Ductal Adenocarcinoma
PD-L1	Programmed death-ligand 1
Pdx-1	Pancreatic and Duodenal Homeobox 1
pH	Potential Hydrogen
PI3K	Phosphoinositide 3-kinase
pLKO	Knockdown vector
pLKO_shGATA6_91	GATA6 Knockdown Vector
pLKO_shGATA6_93	GATA6 Knockdown Vector 2 (another shRNA sequence)
pLKO_shNt	Non-targeting Knockdown Vector
pSPAX2	Packaging Vector
PTEN	Phosphatase and Tensin Homolog
PTHLH	Parathyroid Hormone Like Hormone
Puro	Puromycin
PVSV-G	Envelope Vector
qPCR	Quantitative Polymerase Chain Reaction
R172H	Arginine to Histidine Substitution at Position 172
RIPA	Radioimmunoprecipitation Assay Buffer
RNA	Ribonucleic acid
RNA-seq	RNA-sequencing
RPMI-1640	Roswell Park Memorial Institute (RPMI) 1640 Medium
RT-qPCR	Quantitative Reverse Transcriptase Polymerase Chain Reaction
RUNX3	RUNX Family Transcription Factor 3
S100A2	S100 Calcium-binding Protein A2
SDS	Sodium Dodecyl Sulfate
SEs	Superenhancers
sh91	pLKO_shGATA6_91
SHH	Sonic Hedgehog
shNt	pLKO_shNt
shRNA knockdown	Short Hairpin RNA Knockdown
SMAD4	SMAD Family Member 4
SMF	Single Molecule Footprinting
SNAI1	Snail
SNAI2	Slug
TAp63	transactivation domain p63 isoform
TCGA	The Cancer Genome Atlas
TP53	Tumor Protein 53

TP63	Tumor Protein 63
TWIST1	TWIST Homolog 1
Univ.-Prof.	University Professor
UTY	Lysine Demethylase 6C
UV	Ultraviolet
VIM	Vimentin
ZEB1	Zinc Finger E-box Binding Homeobox 1
ΔNp63	amino-deleted p63 isoform
ΔNp63α	Second Isoform of p63

Table 1: Used abbreviations and their meaning.

12.2 Materials and methods

12.2.1 Cell culture

All experiments were conducted with BXPC3, L3.6 and PaTu8988S (from here on PaTu) established human PDAC cell lines. For lentiviral transduction, HEK293FT cells have been used in addition to the previously stated cell lines. BXPC3 and L3.6 cells were cultured in RPMI-1640 medium, while PaTu and HEK293FT were cultured in DMEM medium. All media had 10% fetal bovine serum and 1x Penicillin-Streptomycin added before handling.

Simplified name	Official cell line name according to Cellosaurus
BXPC3	BxPC-3
HEK293FT	HEK293-FT
L3.6	L3.6pl
PaTu	PaTu 8988S

Table 2: Used cell lines and their official names according to Cellosaurus.

12.2.1.1 Thawing

A cryotube with cells was taken out of the -80°C freezer or the liquid nitrogen tower and normally thawed for 1 minute at 37°C in the water bath. It was important that the thawing step was performed fast since the dimethyl sulfoxide (DMSO), which saves the cells when they are frozen from ice crystal formation, is also cytotoxic to the cells when they are in suspension. Additionally, the suspension should also be immediately diluted to minimize the DMSO effect. Therefore, 5ml of DMEM medium (Sigma-Aldrich, D6429-500ML) or RPMI-1640 medium (Sigma-Aldrich, R8758-500ML) containing 10% fetal bovine serum (FBS) (biowest, S181H-500) and 1x Penicillin-Streptomycin (Sigma-Aldrich, P4333-100ML) were added to the cell suspension, which was subsequently centrifuged to remove the DMSO from the cells. The supernatant was discarded, and the pellet was resuspended in fresh medium. The cell suspension was transferred into a cell culture dish and incubated at 37°C with 5% CO_2 and 92% relative humidity for three to five days until they reached around 80% confluency.

12.2.1.2 Maintenance

The cells were split every three to five days in a 1:3 ratio. This was conducted by discarding the old medium from the cell culture dish and washing with 1xPBS (Sigma-Aldrich, D8537-500ML) at first. Subsequently, trypsin (0.05% Sigma-Aldrich, T4049-100ML) was added to the adherent cells and incubated for five minutes at 37°C to detach them from the culture dish. To stop the reaction, fresh medium containing FBS was added to the cells. The cell suspension was divided and seeded into new cell culture dishes and the additional medium was added to each dish to reach an equal volume. The cells were incubated at 37°C with 5% CO_2 and 92% relative humidity.

12.2.1.3 Freezing

Cells were frozen on a regular basis. This was carried out by centrifuging a part of the cells during the maintenance splits, discarding the supernatant and resuspending in cold FBS, to which 10% of DMSO (Carl Roth, A994.2) was added. Subsequently, the cell suspension was transferred into cryotubes and frozen inside a freezing container at -80°C. The use of the freezing container is critical since it ensures a slow freezing rate of 1°C per minute for the cell suspension. Freezing the cells slowly leads to a slower formation of ice crystals. Together with the use of DMSO, which inhibits ice crystal formation, this procedure makes sure that more cells survive the freezing and thawing process.

12.2.1.4 Counting and seeding

Whenever the cells were to be seeded at a specific density for an experiment, the cell suspension was counted. This was performed by using a Neubauer Improved cell counting chamber and staining the cells with trypan blue, to exclude dead cells. The cell suspension was afterward diluted to fit the cell count for the respective experiment. Then the cell suspension was pipetted into the wells and incubated for at least 24 hours with the same conditions as mentioned before.

12.2.1.5 Proliferation assay

Cells were trypsinized, counted and seeded in triplicates at a density of 30,000 cells per well into 5 6-well plates. The cells were counted on the day after seeding as the reference time point. Afterward, cells were counted for five days every day. The medium was changed on the third day after the seeding of the experiment.

12.2.1.6 Migration/Scratch wound healing assay

Cells were seeded in triplicates at a density of 100,000 cells per well into 12-well plates. When cells reached confluency, the cell monolayer was scratched by dragging a sterile 10µL pipet tip across the well to generate a wound. Afterward, the wells were washed with PBS before adding a medium without FBS. Pictures of the scratches were acquired with a Nikon TE 300 inverted fluorescence phase-contrast microscope immediately, 24 hours and 48 hours post scratch to assess the cells' migratory potential. In between the plates were incubated as usual. The wound areas were quantified with ImageJ 1.52n.

12.2.1.7 Invasion/Transwell Matrigel assay

Transwells were coated with Matrigel at least one day prior to the start of the experiment. Therefore, Matrigel was thawed on ice and diluted 1:10 in cold PBS and 50µL of this mixture was added per transwell. The plate with the transwells was left open overnight in the cell culture hood with turned on UV light to aid the polymerization. On the next morning, the plate was transferred to storage at 4°C.

While preparing the cell suspension in a serum-free medium, the plate was taken out of the fridge and the Matrigel was rehydrated from the inner and the outer compartment with serum-free medium. The medium from the inner and outer compartment was discarded and instead, 100,000 cells per well were seeded into the inner compartment on top of the Matrigel. Afterward medium with serum was added to the outer compartment to stimulate the invasion of the cells into the Matrigel. The samples were collected after 24 or 48 hours. The transwells were washed twice with PBS, fixed with 4% paraformaldehyde for 10 minutes on ice, and washed with PBS twice again. Nuclei of the cells were subsequently stained with DAPI for 10 minutes before an additional PBS wash and removal of the Matrigel from the transwell with a cotton swab. The membrane was dried and cut before mounting on a slide with the cells on the bottom side using Dako Fluorescence Mounting Medium. The slides were dried covered at room temperature overnight before acquiring pictures with an upright FL Nikon Eclipse 80i microscope. Overlapping pictures of the specimen were taken, which were afterward stitched together with ImageJ. The stitched images were afterwards quantified for DAPI-positive nuclei using the Definiens software.

12.2.2 Generation of the overexpression/knockdown cell lines

12.2.2.1 Lentiviral Transduction

Target cells were transduced with lentiviruses produced in HEK293FT cells. For this purpose, the HEK293FT cells were transfected with 10µg of DNA of interest, 8µg of packaging vector pSPAX2 and 3µg of envelope vector pVSV-G. On day 2, the medium of the HEK293FT cells was changed. On day 3, for the infection of the BXPC3 cells, the supernatant of the HEK293FT cells was filtered through a 0.45µm filter to remove any floating cell and avoid cell cross-contamination. BXPC3 cells were repeatedly incubated with filtered fresh supernatant of the HEK293FT cells and the addition of polybrene for a total of 4 infection cycles. Since the overexpression vector contains GFP, on day 5, the cells were checked for GFP expression under a microscope to determine positive transduction. Now the cells were cultured normally since the reverse transcription and integration should take place within 24 to 36 hours post-transduction.

The knockdown vector contains instead of GFP a resistance against the antibiotic puromycin. Therefore, to select only for the knockdown cells, puromycin was added to the medium when culturing the knockdown cells.

Plasmid name	Plasmid purpose
FG12	Empty overexpression vector
FG12-GATA6	GATA6 overexpression vector
pLKO-shNt	Empty knockdown vector
pLKO-shGATA6-91	GATA6 knockdown vector
pLKO-shGATA6-93	GATA6 knockdown vector (another shRNA sequence compared to pLKO-shGATA6-91)
pSPAX2	Packaging vector
pVSV-G	Envelope vector

Table 3: Used plasmids for lentiviral transduction.

12.2.3 Immunofluorescence

Cells were seeded onto coverslips until 80% confluency and fixed with paraformaldehyde. Subsequently, the cells were permeabilized with Triton X-100 and blocked with BSA 5% in PBS. The primary and secondary antibodies were then incubated for 1 hour each at room temperature with washes in between. Before the coverslip was mounted on a slide, the nuclei were stained with DAPI for 10 minutes. The images were acquired using a confocal microscope.

Antibody	Host	Company	Catalog number	Concentration
GATA6	Goat	R&D	AF1700	1:200
p63	Rabbit	GeneTex	GTX102425-100	1:200

Table 4: Used antibodies and the concentration used.

12.2.4 Cell sorting of GFP-positive cells

Transduced BXPC3 cells were trypsinized, centrifuged, resuspended in PBS, and kept on ice for cell sorting. The cells were filtered and sorted for GFP-positive cells, which were recovered. After recovery, the cells were centrifuged and plated in normal medium with antibiotics at double concentration, for one week after sorting.

12.2.5 Comparison of cell proliferation rate with Bromodeoxyuridine

Cells were incubated with 100µM Bromodeoxyuridine (BrdU) for 2 hours at 37°C. Afterward, the cells were fixed with paraformaldehyde. Subsequently, the cells were permeabilized with Triton X-100 and blocked with BSA. When preparing the dilution of the primary antibody, magnesium chloride and DNase were added together with the anti-BrdU antibody. The primary and secondary antibodies were then incubated for 1 hour each at room temperature with washes in between. Before the coverslip was mounted on a slide, the nuclei were stained with DAPI for 10 minutes. The images were acquired using a confocal microscope and positive nuclei were counted manually from at least 5 non-overlapping pictures for each condition.

12.2.6 Cell lysis

When the cells reached about 80% confluency, the cells were lysed by adding Laemmli cell lysis buffer. After 2 washes with cold PBS, the buffer was pipetted directly onto the cells and the whole dish was scraped before transferring the liquid into a tube. The samples were sonicated, a Bradford protein concentration assay was conducted, and the samples were boiled at 95°C for five minutes and stored at -20°C if not loaded onto a gel immediately.

12.2.7 Western Blot

Polyacrylamide gels with an 8% separating and a stacking gel were prepared. After polymerization, a marker (PageRuler Prestained Protein Ladder, Thermo Scientific, #26616) and lysed cell samples were loaded, and the gels were run. Subsequently, the proteins from the gels were transferred to nitrocellulose membranes and checked for successful transfer with Ponceau S. Before antibody incubation the membranes were blocked with 5% milk in TBS-Tween. The primary antibodies were incubated overnight at 4°C. The membranes were washed three times in TBT-Tween, incubated with HRP-conjugated secondary antibodies for 45 minutes at room temperature, and washed again. To develop the blot, chemiluminescence reagents were added directly to the membrane and films were exposed to this chemiluminescence in a dark room before developing the film. The obtained films were scanned, and band intensity was quantified using the ImageJ software.

Antibody	Host	Company	Catalog number	Concentration
E-cadherin	Mouse	BD	610181	1:1,000
GAPDH	Mouse	eBioscience	14-9523-80	1:1,000
GATA6	Goat	R&D	AF1700	1:500
GATA6	Rabbit	Cell Signaling	#5851	1:1,000
Keratin 14	Rabbit	Biolegend	905304	1:1,000
p63	Rabbit	GeneTex	GTX102425-100	1:500
Vinculin	Mouse	Sigma-Aldrich	V9264	1:2,000

Table 5: Used antibodies and the concentration used.

12.2.8 RNA extraction

Cells grown in a monolayer were lysed directly in the 6cm cell culture dish with 1mL peqGOLD TriFast (VWR, 30-2010) by pipetting up and down and transferring the cell suspension to a reaction tube. This cell suspension was either frozen at -80°C or immediately processed. For further processing, the samples were incubated at room temperature for 5 minutes. 0.2mL of chloroform was added, the tubes were vortexed for 15 seconds and afterward incubated for additional 10 minutes at room temperature. The mixture was separated by centrifugation at 12,000xg for 5 minutes and the upper aqueous phase was transferred to another tube. An additional chloroform wash was performed with 500µL to remove residual phenol. The upper phase was precipitated on ice for 15 minutes with 0.5mL of isopropanol. The precipitated RNA was centrifugated at 4°C with 12,000xg for 10 minutes and washed twice with 75% ethanol. Each time the centrifugation was performed as stated above at 4°C with 12,000xg for 10 minutes. The excess of ethanol was removed before letting the pellet air-dry. The dried pellet was resuspended in 50µL of RNase-free water before the RNA concentration was quantified using a NanoDrop microvolume spectrophotometer.

12.2.9 cDNA synthesis

The cDNA synthesis was performed immediately after the quantification of the freshly extracted RNA using the LunaScript RT SuperMix Kit (New England Biolabs, E3010L) according to the protocol. The synthesized cDNA was either used for subsequent RT-qPCR or stored at -20°C until RT-qPCR.

12.2.10 RT-qPCR

Quantitative PCR was performed using a Biorad CFX96 system on 2 µl of cDNA or H_2O which were mixed to 5 µl Luna Universal qPCR Master Mix (New England Biolabs, M3003E), 0.6 µl forward+reverse primers 10 µM, and 2.4 µL H_2O. The PCR program was performed as follows: 60 seconds at 95°C; 40 cycles of 95°C for 15 seconds and 60°C for 30 seconds.

Primer name	Primer sequence (5' to 3')
CDH1_F	AGAACGCATTGCCACATACACTC
CDH1_R	CATTCTGATCGGTTACCGTGATC

CDH2_F	AGATCCTACTGGACGGTTCG
CDH2_R	TCTGCAGCAACAGTAAGGACA
DNP63_ex1-2_F	TGTTGTACCTGGAAAACAATGC
DNP63_ex1-2_R	GAGGAGCCGTTCTGAATCTG
FAT2_ex2-3_F	AGGGAAGCTGACCTTCAACA
FAT2_ex2-3_R	TCATCCTTGTTCTCTCTGTCCA
FOXA1_F	GCTCCAGGATGTTAGGAACTGT
FOXA1_R	ATGGTCATGTAGGTGTTCATGG
FOXA2_F	AGCTACTATGCAGAGCCCGA
FOXA2_R	TACGTGTTCATGCCGTTCAT
GATA6_F	GTGCCCAGACCACTTGCTAT
GATA6_R	TGGAATTATTGCTATTACCAGAGC
HNF4A_ex2-3_F	GGTGCCTCGAGCTGTGAC
HNF4A_ex2-3_R	GGCACTGGTTCCTCTTGTCT
HPRT_F	GGCCAGACTTTGTTGGATTTG
HPRT_R	TGCGCTCATCTTAGGCTTTGT
KLF5_ex3-4_F	AAGCTCACCTGAGGACTCACA
KLF5_ex3-4_R	TAGTGGCGGGTCAGCTCAT
KRT14_ex2-3_F	TCACAGCCACAGTGGACAAT
KRT14_ex2-3_R	ATGTCGGCTTCCACACTCAT
KRT5_ex2-3_F	ACAGCATCGTGGGGGAAC
KRT5_ex2-3_R	TCTCAGCAGTGGTACGCTTG
MYC_ex2-3_1_F	GGATTCTCTGCTCTCCTCGAC
MYC_ex2-3_1_R	ACTCTGACCTTTTGCCAGGA
NECTIN1_ex2-3_F	CTGCGAGTTTGCTACCTTCC
NECTIN1_ex2-3_R	CACTGCCTGGGTACCCTCTA
PTHLH_ex3-4_F	CGGTGTTCCTGCTGAGCTAC
PTHLH_ex3-4_R	AATCGTCGCCGTAAATCTTG
S100A2_ex2-3_F	GGGAAATGAAGGAACTTCTGC
S100A2_ex2-3_R	CCTGCTGGTCACTGTTCTCA
SNAI1_ex1-2_F	GCGAGCTGCAGGACTCTAAT
SNAI1_ex1-2_R	CGGTGGGGTTGAGGATCT
SNAI2_F	ATTTCAACGCCTCCAAAAAG
SNAI2_R	TTGTGGTATGACAGGCATGG
TAP63_ex1-2_F	TTTGAAACTTCACGGTGTGC
TAP63_ex1-2_R	CCATCTTCTGATGGTTCATCC
TWIST1_F	ACCCAGTCGCTGAACGAG
TWIST1_R	TGGAGGACCTGGTAGAGGAA
VIM_F	TCAGAGAGAGGAAGCCGAAA
VIM_R	CAAAGATTCCACTTTGCGTTC

Table 6: Used RT-qPCR primers and their sequence.

12.2.11 Chromatin Immunoprecipitation (ChIP)

Cells were crosslinked with 1% formaldehyde for 10 minutes at room temperature. The reaction was stopped by adding glycine to a final concentration of 0.125M for 5 minutes at room temperature. Fixed cells were washed twice with cold PBS and resuspended in 1mL lysis buffer 1 (50mM Hepes-KOH (pH 7.5), 140mM NaCl, 1mM EDTA, 10% Glycerol, 0.5% Igepal CA-630, 0.25% Triton X-100) supplemented

with protease inhibitors. After rotation for 10 minutes at 4°C followed by centrifugation at 2,000g for 5 minutes at 4°C, the pellet was resuspended in 1mL of lysis buffer 2 (10mM Tris-HCl (pH 8.0), 200mM NaCl, 1mM EDTA, 0.5mM EGTA) supplemented with protease inhibitors. This mixture was again incubated on a nutator for 5 minutes at 4°C. After centrifugation the remaining pellet was resuspended in lysis buffer 3 (10mM Tris-HCl (pH 8.0), 100mM NaCl, 1mM EDTA, 0.5mM EGTA, 0.1% Na-Deoxycholate, 0.5% SDS) and sonicated for 15 minutes (30 sec on/30 sec off/high) in a Diagenode water bath-sonicator and centrifuged at 17,000g for 15 minutes. The cleared supernatant was used for the subsequent chromatin pulldown. For this purpose, the sonicated chromatin was diluted with dilution buffer (1% Triton X-100, 2mM EDTA (pH 8.0), 150mM NaCl, 20mM Tris-HCl (pH 8.1)) supplemented with protease inhibitors, before overnight incubation with the H3K27ac specific antibody and rabbit IgG as an isotype control. The beads were prepared by blocking with BSA in PBS and incubation for 1 hour rotating at room temperature to bind with the respective antibody. The pulldown was achieved by rotation overnight at 4°C with diluted sonicated chromatin and bead-bound antibodies. The beads were then washed six times with ice-cold RIPA buffer (50mM Hepes (pH 7.6), 1mM EDTA, 0.7% Na-Deoxycholate, 1% Igepal CA-630, 0.5M LiCl) and once with TE (10mM Tris (pH 8.0), 10mM EDTA (pH 8.0)). To elute and reverse-crosslink 500µL of elution buffer (1% SDS, 0.1M $NaHCO_3$) and 20µL of 5M NaCl was added to the beads. The incubation was carried out at 65°C for a minimum of 4 hours. To extract only DNA, the mixture was digested by proteinase K before conducting phenol-chloroform extraction.

12.2.12 Phenol-Chloroform extraction

After the proteinase K digestion, the mixture was centrifuged at top-speed for 1 minute at room temperature to pellet down the beads. The supernatant was mixed with 500µL of Phenol-Chloroform-Isoamylalcohol (25:24:1) (Sigma-Aldrich, P2069-400ML) and subsequently vortexed until a white emulsion formed to increase the surface area for better extraction of the DNA. After performing centrifugation at top-speed for 5 minutes at room temperature, 500µL of chloroform was added to the upper phase and the mixture was again vortexed and centrifuged with the prior settings. The DNA was precipitated by adding 500µL of isopropanol and 50µL of 3M NaAc to the upper phase. The tubes were incubated for at least 30 minutes at -20°C prior to top-speed centrifugation for 20 minutes at 4°C. The isopropanol was discarded, and the pellet was washed with 500µL of 70% ice-cold ethanol. This mixture was centrifugated again for 5 minutes at 4°C, prior to the removal of the ethanol and air-drying of the pellet for around 15 minutes at room temperature. The pellet was resuspended in 50µL for ChIP samples and 500µL for the input before storage at -20°C or immediate further processing.

12.2.13 ChIP-qPCR

Specific primers were designed for various genes. The input DNA pulled down from the ChIP was diluted 10 times before qPCR. Quantitative PCR was performed using a Biorad CFX96 system on 2 µl of DNA or H_2O which were mixed to 5 µl Luna Universal qPCR Master Mix (New England Biolabs, M3003E), 0.6 µl forward+reverse primers 10 µM, and 2.4 µL H_2O. The PCR program was performed as follows: 60 seconds at 95°C; 40 cycles of 95°C for 15 seconds and 60°C for 30 seconds.

Primer name	Primer sequence (5' → 3')
DNp63_F	TCCATTGGAGTGGAGGAGTC
DNp63_R	AACAGAACTCAAGTCCCTCTCTC
FAT2-3.7_F	TTCTTTCCTCCTGACTGTGCTTC
FAT2-3.7_R	GTTGAACAGGTAGCAAGTGGTAGA
GATA6 TSS_F	TACTGCTCTGCCGGAAAACT
GATA6 TSS_R	GCAGTTCCGACCCACAGC
HNF4A_TSS_F	CCCTCGGTTTTCCCACTACT
HNF4A_TSS_R	AACCCAGAGCCAGGTGTATG
KRT14_TSS_F	AGGTGGTCATGGTGCAGAG

KRT14_TSSb_R	ATGAAAGCCAAGGGGAATG
KRT5_TSS_F	CTGCCCTTTGACCTTTTCCT
KRT5_TSS_R	AGAGCTTGCTGGAACACACC
NECTIN+31.8_F	GTATCTGTGCTTCCTGCTTCC
NECTIN+31.8_R	GGAGATTCTGAGTGCCTGGT
NEG_F	CATTGGGAAGTGATGATGTGATCT
NEG_R	GTCCTCTCTGCCATCTTCACTCA
PTHLH-50_F	ACGGTCACGGCTCACTGTAT
PTHLH-50_R	AAGTAGCCTGGGCAACATAGG
TAp63_TSS_F	AATCAAGAAACGCTCCGCCT
TAp63_TSS_R	CGGGAGGCTAAAAGCAATAGG

Table 7: Used ChIP-qPCR primers and their sequence.

12.3 List of figures

12.4 List of tables